Nd^{3+}/Yb^{3+} doped BaY_2F_8 microparticles for ratiometric temperature sensing

Oleynikova, E.I[1]*., Rakhmatullin R.M[1].,

Aglyamov R.D[2,1]., Naumov A.K[1,2]., and Pudovkin M.S[1]**

[1]*Kazan Federal University, Institute of physics, 18 Kremlyovskaya str, Kazan, 420008, Russian Federation*

[2]*Zavoisky Physical-Technical Institute, FRC Kazan Scientific Center of RAS, Sibirsky Trakt Str. 10, Kazan, 420029, Russian Federation*

Corresponding authors:

*Oleynikova, E.I: kate15-05@mail.ru

**Pudovkin M.S: jaz7778@list.ru

Keywords

Luminescent thermometry, optical temperature sensing, Nd^{3+}/Yb^{3+}, BaY_2F_8, Stark peaks

Highlights

BaY_2F_8:Nd^{3+}(0.5%)/Yb^{3+} (0.75, 1.0 and 4.0 %) microparticles demonstrated an efficient Nd^{3+} - Yb^{3+} under Nd^{3+} excitation at 790 nm

Temperature sensing based on Nd^{3+} to Yb^{3+} intensity ratio showed competitive $S_r \sim 0.2\ \%\cdot K^{-1}$ at 80 K

Temperature sensing based on the highest Stark of Nd^{3+} to the lowest one of Yb^{3+} intensity ratio showed higher $S_r \sim 1.8\ \%\cdot K^{-1}$ at 80 K

Abstract

We presented experimental results of the spectral-kinetic characterization of $BaY_2F_8:Nd^{3+}$ (0.5 %)/Yb^{3+} (0.75, 1.0, and 4.0 at. %). Using the EPR spectroscopy it was found, that the presence of clustering of Yb^{3+} ions. The luminescence intensity ratio (LIR) of Nd^{3+} ($^4F_{3/2}$ – $^4I_{9/2}$ transition) and Yb^{3+} ($^2F_{5/2}$ – $^2F_{7/2}$ transition) were taken. The maximal $S_r = 0.2\ \%\cdot K^{-1}$ was achieved for $BaY_2F_8:Nd^{3+}$ (0.5 %)/Yb^{3+} (0.75 %) sample. We calculated the LIR of Nd^{3+} and Yb^{3+} Stark peaks. The maximum S_r value was $1.8\ \%\cdot K^{-1}$ at 80 K using $BaY_2F_8:Nd^{3+}$ (0.5 %), Yb^{3+} (0.75 %) sample.

Introduction

Luminescence thermometry is a powerful tool for measuring temperature remotely with submicron spatial resolution. This method is highly required for temperature mapping of microcircuits, detection of temperature within living cells, and for hyperthermia [1], [2], [3], [4], [5]. In the luminescence thermometry, the luminescent phosphors are utilized as probes. In turn, the luminescence signal should be dependent on temperature. In the case of biomedical applications, the optical excitation and luminescence detection should be in the near-infrared spectral range in the so-called "biological window" which defines the range of wavelengths from 650 to 1350 nm where light has its maximum depth of penetration in tissue. For example, the Er^{3+}/Yb^{3+} doped up-conversion phosphors are suitable for such tasks [6], [7] In addition, it also allows eluding undesirable cell autofluorescence in the *in vitro* experiments.

Luminescence thermometry based on Nd^{3+} and Nd^{3+}/Yb^{3+} doped inorganic phosphors is considered a very promising area of temperature sensing due to the high temperature sensitivities, the opportunity to operate in the "biological window", and the capability to manipulate the thermometric performances via the doping ion concentrations (in the case of the double-doped Nd^{3+}/Yb^{3+} systems) [8], [9], [10], [11], [12]. Indeed, Nd^{3+} has several intense absorption bands in ultraviolet, visible, and infrared spectral ranges. In the Nd^{3+}/Yb^{3+} ion pair, usually, Nd^{3+} serves as an energy donor populating the Yb^{3+} ion. The energy transfer occurs via $^4F_{3/2}$ (Nd^{3+}) and $^2F_{5/2}$ (Yb^{3+}) as well as via cross-relaxation ($^4G_{9/2} - {}^4F_{3/2}$ for Nd^{3+}) and ($^2F_{7/2} - {}^2F_{5/2}$ for Yb^{3+}) [13]. The $^4F_{3/2}$ (Nd^{3+}) - $^2F_{5/2}$ (Yb^{3+}) energy transfer is phonon-assisted which paves the way toward temperature sensing based on the analysis of both I_{Nd}/I_{Yb} luminescence intensity ratio (LIR) and luminescence decay times. In the case of the Nd^{3+}/Yb^{3+} system, there are also Yb^{3+} - Nd^{3+} back energy transfer, and energy diffusion between Yb^{3+} ions [13], [14]. The up-conversion materials based on this ion pair are also used in luminescence thermometry [15].

I.V. Barbosa et al. [16] investigated the Nd^{3+}/Yb^{3+} system in a series of oxide hosts (Y_2O_3, YAG, $Y_2Ge_2O_7$, YBO_3, and Y_3BO_6). These hosts differ from each other

by symmetry and phonon energy. One of the most important conclusions of this work is, that the higher absolute temperature sensitivity was achieved for the host with the lowest phonon energy. On the other hand, it is well known, that fluoride hosts demonstrate lower phonon energy compared to some oxide hosts [17]. Moreover, some fluoride materials (LnF_3, Ln = lanthanides, $LiYF_4$, BaY_2F_8) demonstrate good transparency, chemical and mechanical stability, as well as low cytotoxicity [18], [19], [20]. The Nd^{3+}/Yb^{3+} ion pair is relatively well studied in such fluoride hosts as YF_3 [21], LaF_3 [22], and $NaYF_4$ [23]. On the other hand, this ion pair is significantly less studied in BaY_2F_8 host. In turn, BaY_2F_8 is a very promising host for quantum electronics and sensing. Moreover, this host displayed bright luminescence of Ce^{3+} and Nd^{3+} under X-ray excitation [24]. Since X-ray irradiation is capable of traveling through biological tissues, it paves the way toward effective bioimaging and temperature sensing.

In the case of ratiometric temperature sensing for double-doped down-conversion phosphors, the ratio of intensities of donor to acceptor is used. Particularly, for Nd^{3+}/Yb^{3+} ion pair, the LIR between $^4F_{3/2} - {}^4I_J$ (Nd^{3+}) and $^2F_{5/2} - {}^2F_{7/2}$ (Yb^{3+}) is used [16], [25]. For Tm^{3+}/Yb^{3+} ion pair the LIR between $^3H_4 - {}^3H_6$ (Tm^{3+}) and $^2F_{5/2} - {}^2F_{7/2}$ (Yb^{3+}) demonstrated competitive values [26]. In turn, in Pr^{3+}/Yb^{3+} ion pair the LIR between $^1G_4 - {}^3H_4$ (Pr^{3+}) and $^2F_{5/2} - {}^2F_{7/2}$ (Yb^{3+}) emission peaks is taken [27]. The temperature sensitivity of the double-doped down-conversion phosphors is determined by many factors including the energy gap (ΔE) between energy exchanging levels, the phonon energy, the concentrations of the ions, the probabilities of energy diffusion between homonymous ions, etc. It is quite difficult to find an optimal ratio between these processes in order to maximize the temperature sensitivity. On the other hand, for the above-mentioned single-doped phosphors based on the Boltzmann law, the relative temperature sensitivity is determined as $S_r = \Delta E/k_B \cdot T$, where k_B and T are Boltzmann constant and the absolute temperature, respectively. There is only one parameter ΔE. However, it is very difficult to manipulate the energy gap between the energy levels in the 4f electron shell of doping ions due to it is shielded by the higher electron shells ($5s^5$, $5p^6$, and $6s^2$ for

rare-earth ions). For the single-doped ions, the LIR is calculated for two emissions corresponding to the energy levels sharing their populations according to the Boltzmann law [5]. Here, for Pr^{3+} doped phosphors, LIR for the emissions from $^3P_1$ and $^3P_0$ states is taken. For Nd^{3+} single-doped phosphors, the LIR is usually calculated between two Stark components of the $^4F_{3/2}$ excited state. Here, the relative temperature sensitivity is determined by ΔE between the above-mentioned levels.

In the present work, we present a slightly combined approach. Indeed, in the BaY_2F_8 host, the Stark components of both Nd^{3+} and Yb^{3+} are resolved well especially at temperatures lower than 200 K. Here, we calculate the LIR between the highest Stark peak of Nd^{3+} and the lowest one of Yb^{3+} in order to enlarge the energy gap between the studied levels. In no uncertain terms, that this energy gap does not determine the relative temperature sensitivity because we consider the levels of different ions. However, this approach can be useful for temperature sensing applications. In order to investigate a physical mechanism of luminescence temperature sensitivity, we carried out a thorough spectral-kinetic characterization. In addition, we paid attention to electron paramagnetic resonance characterization of the samples because this method allows making conclusions about the type of paramagnetic centers and implicitly conclude about the presence of ion clusters. Indeed, in clusters the luminescence quenching is more effective which can affect the temperature sensitivity.

The objective of this research was a physical characterization of the BaY_2F_8:Nd^{3+}/Yb^{3+} in order to conclude about the possibility of the use of these materials in temperature sensing.

The tasks were:

- synthesis of BaY_2F_8:Nd^{3+}/Yb^{3+} microparticles;

- physical characterization of the samples via X-ray diffraction (XRD), electron paramagnetic resonance, and laser spectroscopy;

- spectral-kinetic characterization at different temperatures;

- calculation of such important characteristics as absolute and relative temperature sensitivities, and temperature uncertainly.

Materials and methods

$BaY_2F_8:Nd^{3+}/Yb^{3+}$ bulk crystals were grown by vertically directed crystallization method from pre-synthesized batch components. The growth was carried out in an active (fluorinating) argon atmosphere at a temperature of 950 °C. All initial batch components had a purity of at least 99.99%. To obtain doped crystal samples, NdF_3 compounds were introduced into the batch in an amount of 0.5 at.%, Some samples were additionally co-activated by introducing YbF_3 compounds into the batch in an amount of 0.75, 1.0, and 4.0 at.%. During the growth process, the crucible with the melt was moved through a zone with a temperature gradient of at least 120 C°/cm at a speed of 2 mm/hour. The grown samples had high optical quality, no visible defects, no scattering of the control laser radiation, and were conical in shape with an average diameter of 8 mm and a length of 35–40 mm. Then, the crystals were mechanically milled in agar mortar in order to obtain a homogenous powder. In order to maintain uniformity, we took the same parts of the crystals for the milling procedure. The doping ion concentrations are presented in atomic percentages. The values of the concentrations form the ratio of the starting materials.

The phase composition of the obtained powders was studied via the conventional X-ray diffraction method (XRD). We used Bruker D8 Advance X-ray diffractometer (Cu K_α radiation with wavelength λ = 0.154 nm). The XRD pattern simulation was performed using VESTA software [28].

The EPR measurements were carried out using continuous wave spectrometer Bruker ESP-300, operating at X-band (~9.4 GHz). The standard modulation frequency was 100 kHz, the modulation amplitude 5 G, the typical power level was 10 mW. Low temperatures were obtained with a commercial liquid-helium flow cryostat system (Oxford Instruments).

The luminescence spectra were recorded using (StellarNet) CCD spectrometer (~1 nm spectral resolution). The samples were optically excited by an infrared laser diode (λ_{exc} = 790 nm, which corresponds to the $^4I_{9/2}$ - $^4F_{5/2}$ absorption band of Nd^{3+} ion). The pulse duration and period were 5 ms and 30 ms, respectively. The spectral characterization was carried out in the 80–320 K temperature range using the “cold

finger” method using a CRYO Industries cryostat with a LakeShore Model 325 temperature controller (USA). Liquid nitrogen was used as a cooling agent. The luminescence decay curves were recorded using a BORDO 211 A digital oscilloscope (bandwidth 10 bits, 200 MHz), MDR-3 monochromator, and PEM-62 photomultiplier (operating spectral range ~ 600–1200 nm).

Results and discussion

The XRD patterns of the doped BaY_2F_8 samples and the VESTA simulation of the BaY_2F_8 host are presented in **Figure 1**.

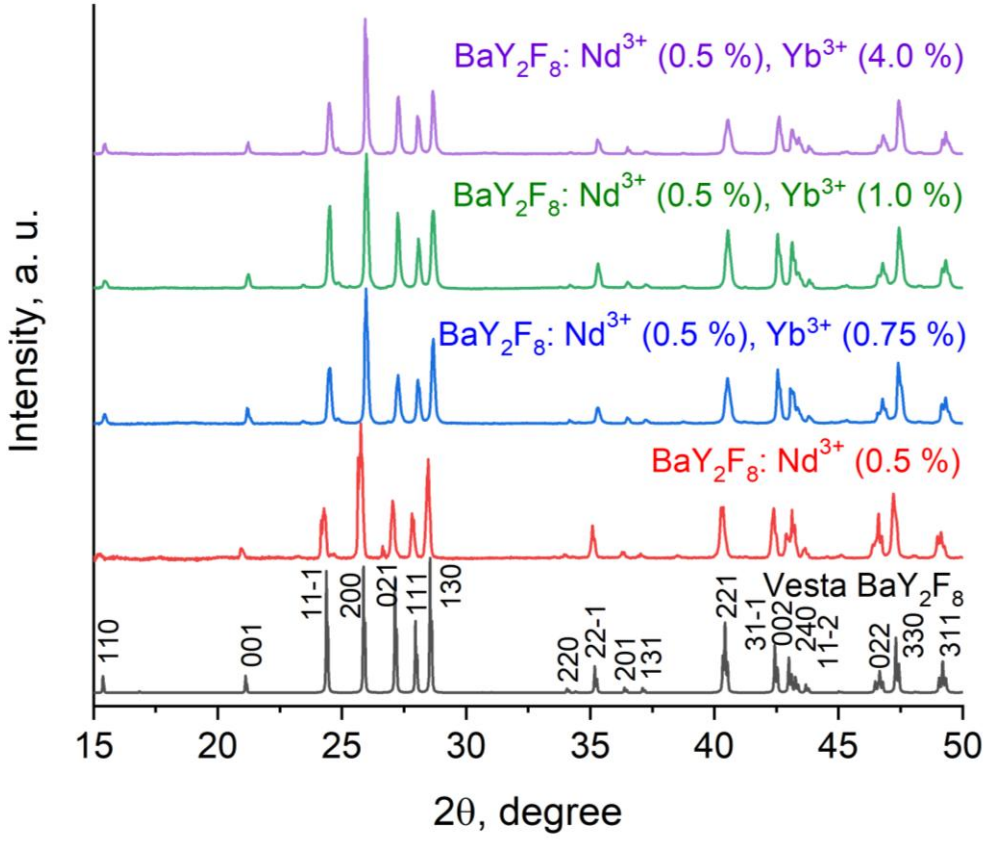

Figure 1. The XRD patterns of the BaY_2F_8:Nd^{3+}/Yb^{3+} samples and the VESTA simulation

All XRD peaks were interpreted as the peaks corresponding to the phase of BaY_2F_8 which has a monoclinic crystal structure. The obtained results are in accordance with the literature data [29], [30], [31] as well as with the VESTA simulation. The simulation of BaY_2F_8 lattice cell carried out via VESTA software is presented in **Figure 2**.

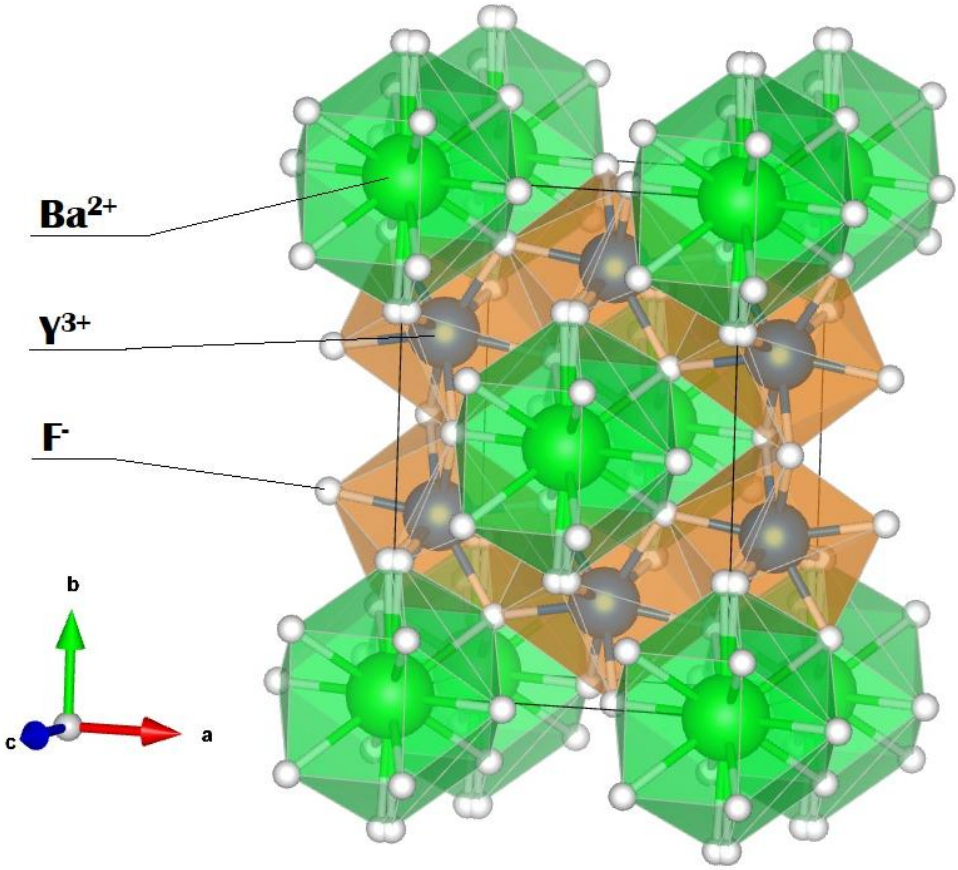

Figure 2. The simulation of BaY_2F_8 lattice cell performed via VESTA software

Since we milled the bulk crystal for around several minutes. We do not expect the nano-sized particles. The optical microscope image of the particles is presented in **Figure S1** of the Supplementary file. The particles can be classified as microparticles. As we mentioned above, the EPR measurements of BaY_2F_8 microparticles were conducted to determine whether clustering of the double-doped Nd^{3+}/Yb^{3+} rare-earth ions occurs. Since we have a sample doped solely with Nd^{3+} ions, its EPR spectrum, presented in **Figure 3**, helps us to interpret the more complex EPR spectra of the Nd^{3+}/Yb^{3+} double-doped powder. The intense lines in **Figure 3** are due to even isotopes of Nd^{3+} ions, while the weaker lines are a hyperfine structure due to odd isotopes (Nd^{143}, 12.2% abundance; Nd^{145}, 8.3% abundance). The measured g-values are collected in **Table 1** along with the g-values, known from the literature [32]. It is worth noting that EPR of Nd^{3+} and Yb^{3+} ions in the BaY_2F_8 crystals was

studied in the past by I.N. Kurkin et al. [32] at four microwave frequencies, 9, 24, 37 and 71 GHz, at liquid helium temperatures. They found from the angular dependencies of EPR spectra that the doping rare-earth ions occupy the single-type centers and they are

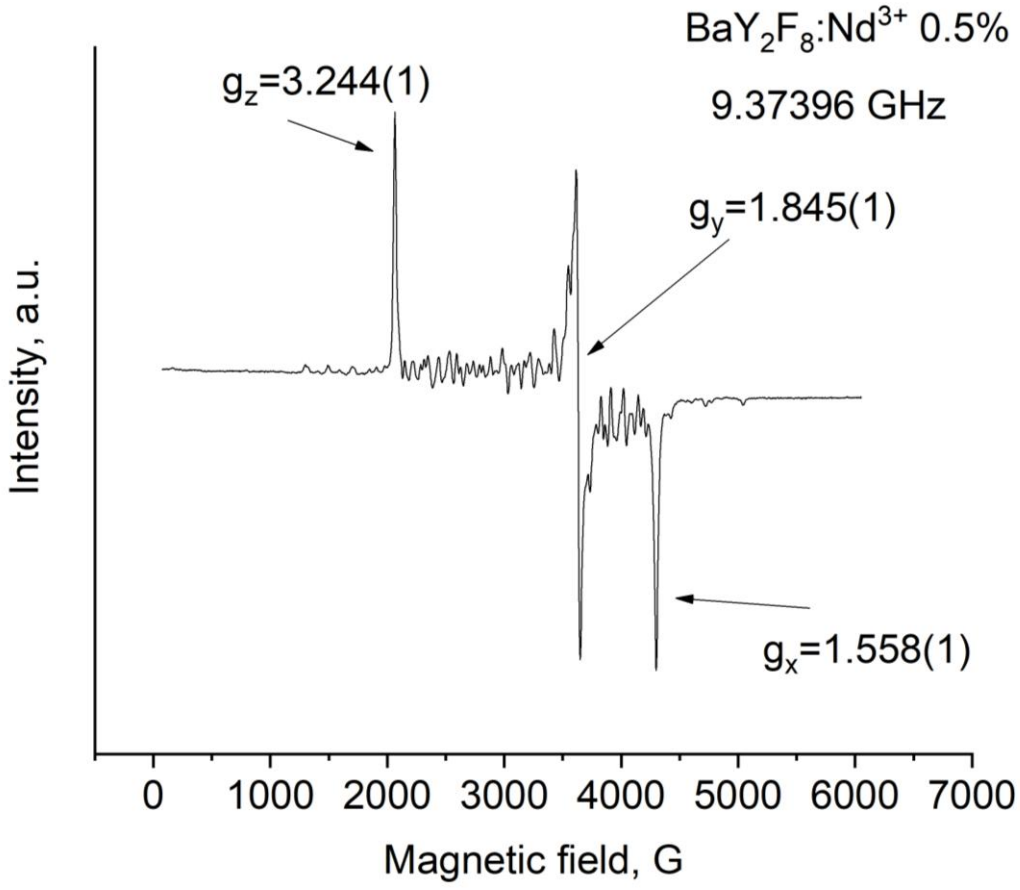

Figure 3. The powder EPR spectrum of Nd^{3+} (0.5 %) ions in BaY_2F_8, microwave frequency 9.37396 GHz, temperature 15 K. Small intensity lines are due to hyperfine structure of odd isotopes of Nd^{143} and Nd^{145} ions

magnetic equivalent. It was supposed that doping rare-earth ions replace the Y^{3+} positions, which are surrounded by 8 fluorine ions and have C_2 local symmetry. Notably, the g-values reported by I.N.Kurkin et al. are in excellent agreement with those obtained in the present study for Nd^{3+} ions in the BaY_2F_8 powder sample.

Figure 4 presents experimental EPR spectra of double-doped BaY_2F_8:Nd^{3+} (0.5 %)/Yb^{3+} (0.75%) powder measured at 300, 40, and 15 K. This plot shows that EPR spectra are detectable only at low temperatures which are typical for the rare-earth

Nd^{3+} and Yb^{3+} ions [33]. Note, that at 40 K, only the EPR lines from Yb^{3+} ions are observable, while those from Nd^{3+} ions have disappeared. The measured g-values for Yb^{3+} ions are collected in **Table 1**.

Table 1. The g-values of isolated Nd^{3+} and Yb^{3+} ions in BaY_2F_8 host.

Ion	g_x	g_y	g_z	References
Nd^{3+}	1.566(2)	1.851(3)	3.277(5)	Kurkin et al [32]
	1.558(1)	1.845(1)	3.244(1)	This work
Yb^{3+}	1.994(3)	2.063(3)	5.049(8)	Kurkin et al [32]
	undefined	2.086(1)	5.077(1)	This work
	1.61	3.34	5.09	designated as $g_{\|\|}$ in [34]
	1.73	3.34	4.91	designated as $g_{\perp}$ in [34]

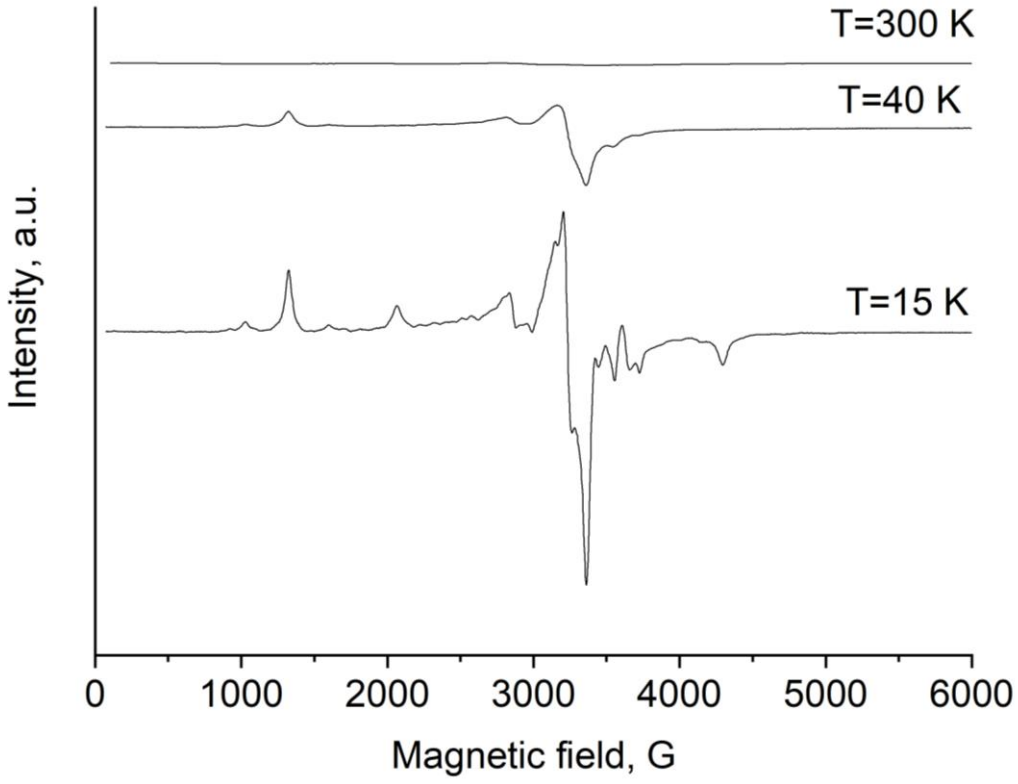

Figure 4. The powder EPR spectra of double-doped BaY_2F_8:Nd^{3+}(0.5 %)/Yb^{3+} (0.75%) sample at 15, 40 and 300 K

To understand the powder EPR spectra of double-doped BaY_2F_8 samples, we made the simulations which are shown in **Figure S2, and Figure S3,** (supplementary information) along with the experimental EPR spectra of BaY_2F_8:Nd^{3+}/Yb^{3+} powder. The simulations were made using EasySpin [35] software package with the following g-values. Nd^{3+}: g_x =1.5579, g_y = 1.84474, g_z = 3.2445; Yb^{3+}: g_x =1.994, g_y = 2.063, g_z = 5.049. The simulation shows that no pairs of Yb^{3+} or Nd^{3+} ions were detected at the concentration of 0.5%Nd and 0.75%Yb. EPR spectra of samples with the higher concentration of Yb^{3+} ions are shown in **Figure 5**. In this plot, the line with g~2.34 is significantly increased compared to other components of the spectra for the sample, containing 0.5%Nd^{3+}, 4%Yb^{3+} ions. This can be an indication of the detectable number of pairs of Yb^{3+} ions in the sample. Recently, S.M. Kaczmarek et al. [34] carried out an experimental study of the BaY_2F_8 crystal doped with 10 mol.% of Yb^{3+} ions and measured the g-values for the single Yb^{3+} ions and pairs.

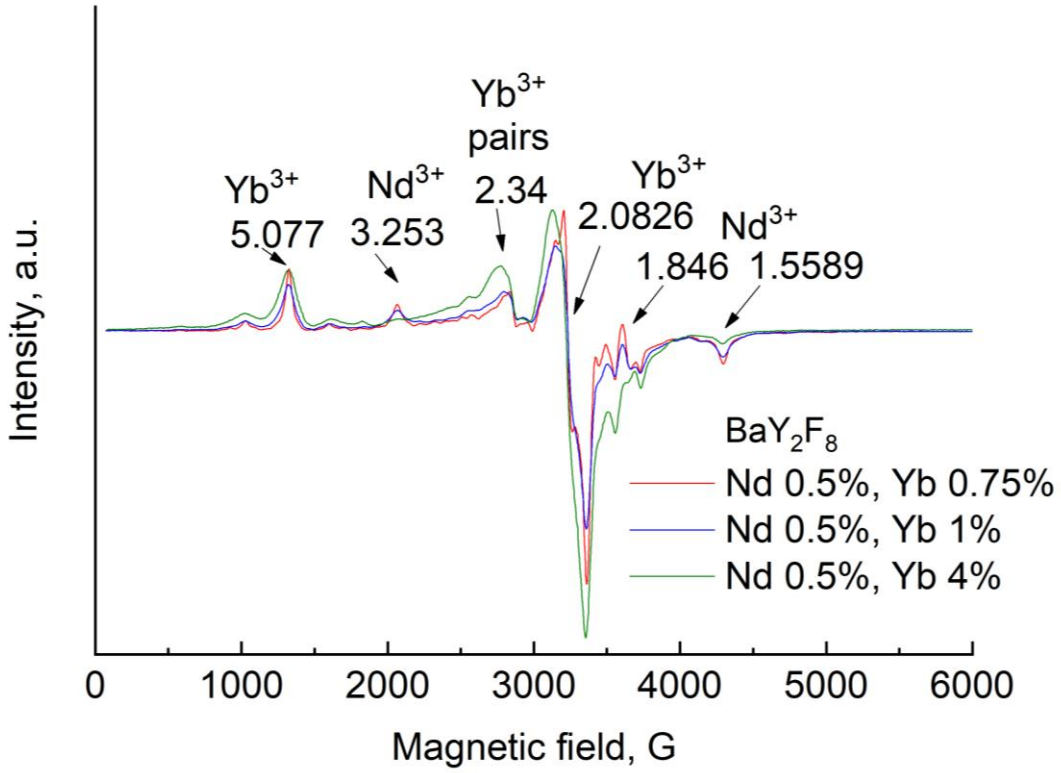

Figure 5. The powder EPR spectrum of double-doped BaY_2F_8:Nd^{3+} (0.5 %)/Yb^{3+} (0.75; 1.0; 4.0 %) (the microwave frequency of 9.37674 GHz), temperature 15 K. Figures designate g-values of corresponding ions

The lines assigned to the pairs of Yb^{3+} ions in a publication by S.M. Kaczmarek et al have g-values of 2.216 ($g_{||}$) and 2.241($g_{\perp}$). These values are comparable to the g-value measured in the present work taking into account a big difference in concentration of doped ions and a difference between powder and crystalline samples. Note, that g-values of isolated Yb^{3+} ions obtained in ref. [34], given for comparison in **Table 1,** are quite different from our values, probably due to big difference in concentration of doped ions or the growth technique of crystals.

Finally, according to the EPR characterization, at 4.0 % of Yb^{3+} these ions form pairs or even clusters. Here, the energy diffusion between Yb^{3+} occurs more effectively.

After the confirmation of the phase composition and EPR characterization, the spectral-kinetic characterization of the samples should be conducted. An energy level diagram of the Nd^{3+}/Yb^{3+} system is presented in **Figure 6**.

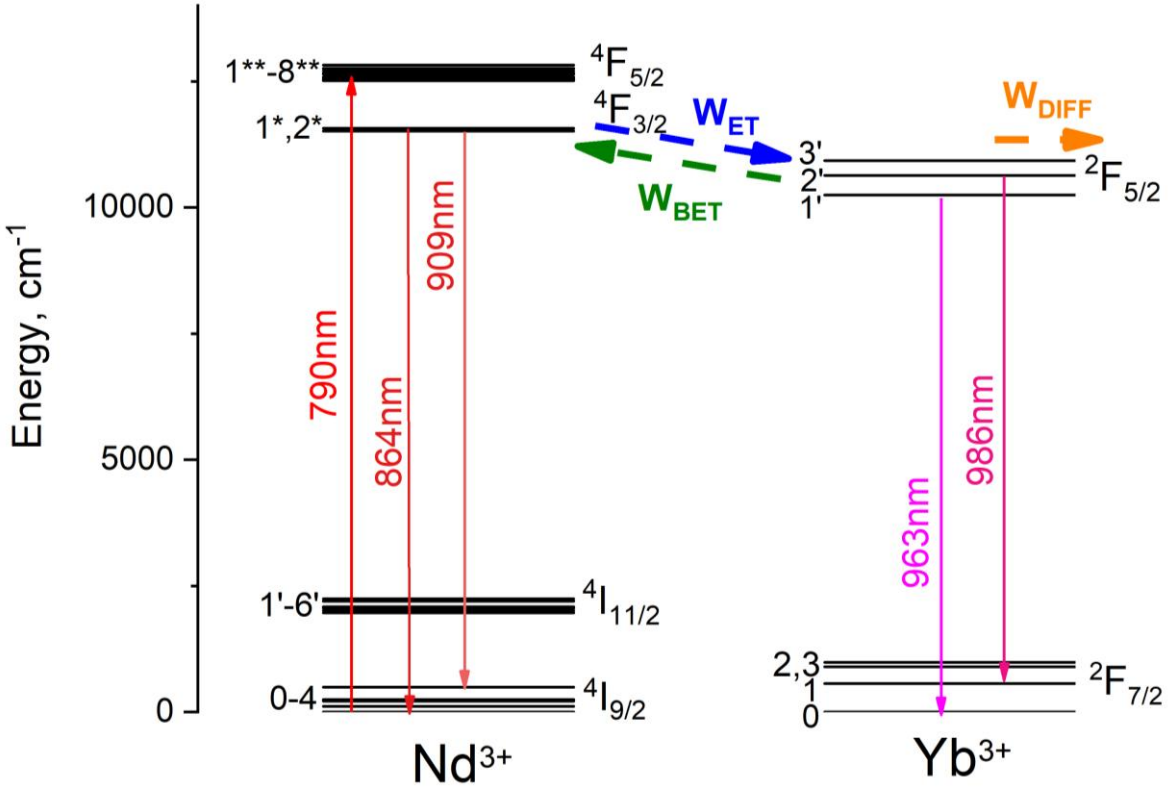

Figure 6. Energy level diagram of the Nd^{3+}/Yb^{3+} system. There are three energy exchange processes which are determined by their probabilities W: Nd^{3+} - Yb^{3+} energy transfer (W_{ET}), Yb^{3+} - Nd^{3+} back energy transfer (W_{BET}), and energy diffusion between Yb^{3+} ions (W_{DIFF}). In the case of Nd^{3+} ion, the $^4F_{3/2}$ level is split to two Stark levels (here, the 2* one is the highest)

Figure 6 illustrates at least three energy exchange processes which are determined by their probabilities W: Nd^{3+} - Yb^{3+} energy transfer (W_{ET}), Yb^{3+} - Nd^{3+} back energy transfer (W_{BET}), and energy diffusion between Yb^{3+} ions (W_{DIFF}). In turn, W_{BET} and W_{DIFF} are competitive. In particular, when the W_{DIFF} increases (with the increase of Yb^{3+} concentration) the W_{BET} decreases, because the resonant Yb^{3+} - Yb^{3+} energy transfer has higher probability [25].

The normalized room temperature luminescence spectra of BaY_2F_8: Nd^{3+} (0.5 %), Yb^{3+} (0, 0.75, 1.0, and 4.0%) microparticles are presented in **Figure 7**. The Stark peaks were also identified according to the literature data [36], [37].

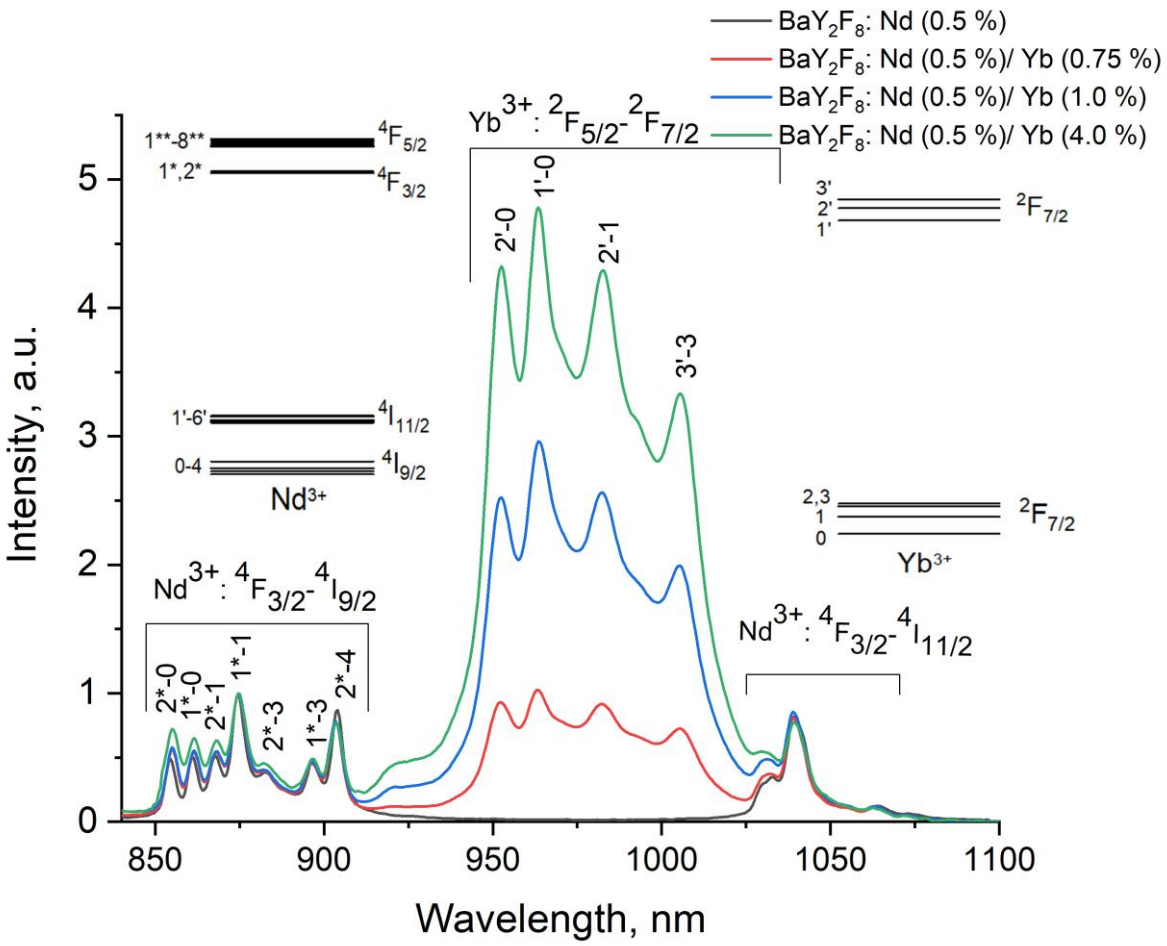

Figure 7. The normalized room temperature luminescence spectra of BaY_2F_8:Nd^{3+} (0.5 %)/Yb^{3+} (0.75, 1.0, and 4.0 %) microparticles normalized at 875 nm Stark peak of Nd^{3+}. Excitation wavelength 790 nm corresponds to the $^4I_{9/2} – {}^4F_{5/2}$ absorption band of Nd^{3+}

It can be seen, that under Nd^{3+} excitation, the intense Yb^{3+} emission is clearly observed which indicates an effective energy transfer from Nd^{3+} to Yb^{3+}. The Yb^{3+} intensity increases compared to Nd^{3+} one with the increase of Yb^{3+} concentration, which is expected for such down-conversion systems. In addition, the intensities of both Nd^{3+} and Yb^{3+} are well separated and have comparable intensity values which is very convenient for ratiometric (I_{Nd}/I_{Yb}) temperature sensing.

The luminescence decay time curves of BaY_2F_8:Nd^{3+} (0.5 %)/Yb^{3+} (0.75, 1.0, and 4.0 %) microparticles are presented in **Figure 8.** Here, the excitation wavelength 790 nm corresponds to the $^4I_{9/2} – {}^4F_{5/2}$ absorption band of Nd^{3+}. In turn, the emission wavelength 909 nm corresponds to $^4F_{3/2} – {}^4I_{9/2}$ transition of Nd^{3+} ions. Here, the

excitation wavelength 790 nm corresponds to the $^4I_{9/2} - {}^4F_{5/2}$ absorption band of Nd^{3+}. In turn, the emission wavelength 909 nm corresponds to $^4F_{3/2} - {}^4I_{9/2}$ transition of Nd^{3+} ions.

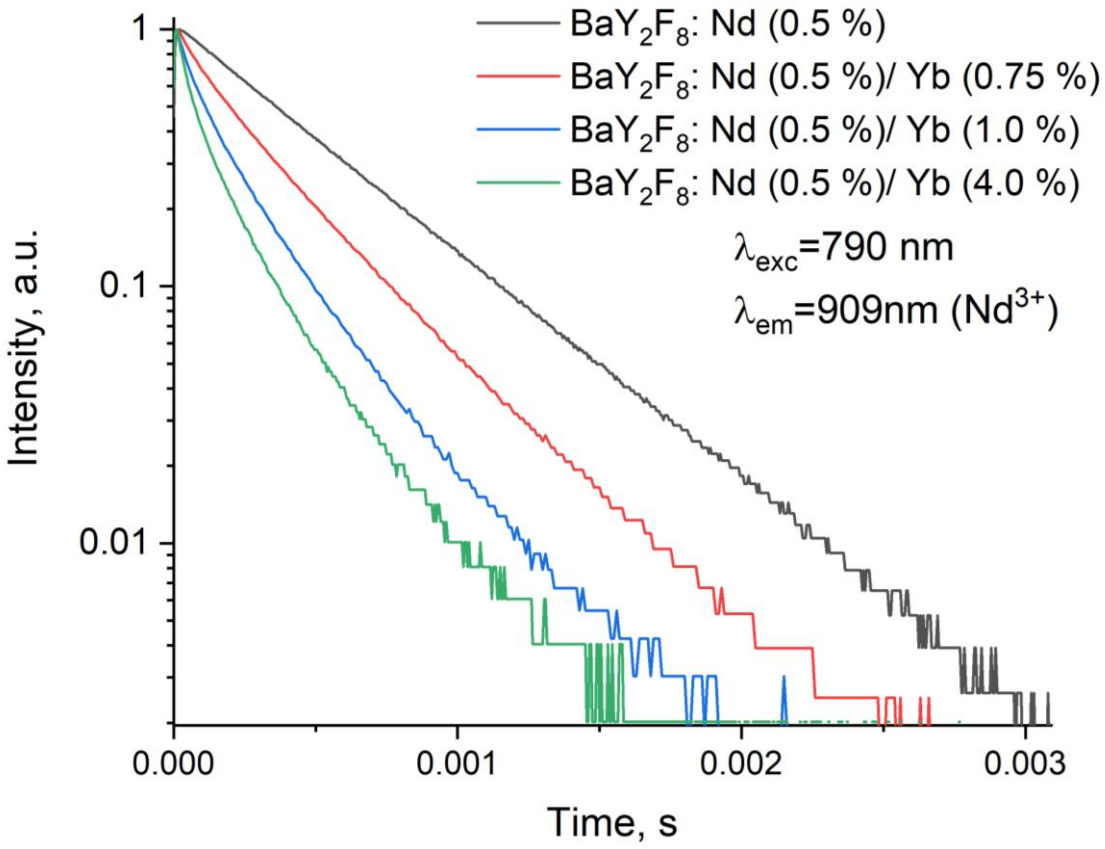

Figure 8. The luminescence decay time curves of $BaY_2F_8:Nd^{3+}$ (0.5 %)/Yb^{3+} (0.75, 1.0, and 4.0 %) microparticles. Here, the excitation wavelength 790 nm corresponds to the $^4I_{9/2} - {}^4F_{5/2}$ absorption band of Nd^{3+}. In turn, the emission wavelength 909 nm corresponds to $^4F_{3/2} - {}^4I_{9/2}$ transition of Nd^{3+} ions

It is seen, that the rate of decay of the luminescence intercity increases with the increase of Yb^{3+} concentration. We also calculated the energy transfer coefficient according to the formula:

$$K = \left(1 - \frac{\tau_{Nd,Yb}}{\tau_{Nd}}\right) * 100\%, \quad (1)$$

Since, the decay curves are not single-exponential (except for single-doped $BaY_2F_8:Nd^{3+}$ (0.5 %), we used a conventional equation:

$$\tau = \frac{\int_0^\infty tI(t)dt}{\int_0^\infty I(t)dt}, \qquad (2)$$

The obtained results are listed in **Table 2.**

Table 2 - Effective decay times and energy transfer efficiency values

Sample	Effective decay times Nd^{3+} ($^4F_{3/2}$ – $^4I_{9/2}$ transition at 909 nm), μs	Energy transfer efficiency values, %	Effective decay times Yb^{3+} ($^2F_{5/2}$ – $^2F_{7/2}$ transition, 963 nm) ms
Nd^{3+} (0.5 %):BaY_2F_8	487.9	-	-
Nd^{3+} (0.5 %), Yb^{3+} (0.75 %):BaY_2F_8	361.5	25.9	2.04
Nd^{3+} (0.5 %), Yb^{3+} (1.0 %):BaY_2F_8	271.2	44.4	1.97
Nd^{3+} (0.5 %), Yb^{3+} (2.0 %):BaY_2F_8	230.7	52.7	2.06

We compared the lifetime of $^4F_{3/2}$ excited state Nd^{3+} in BaY_2F_8 host . For example, ref. [10] reports, that the radiative lifetime of the $^4F_{3/2}$ excited state at 300 K is equal to 470 μs. This value is in good agreement with the single-doped BaY_2F_8:Nd^{3+}.

The luminescence spectra of BaY_2F_8:Nd^{3+} (0.5%)/Yb^{3+} (0.75, 1.0, and 4.0%) microparticles in the 100 – 300 K temperature range normalized at 875 nm Stark peak of Nd^{3+} are presented in **Figure 9.** The excitation wavelength λ_{ex} = 790 nm corresponds to the $^4I_{9/2}$ – $^4F_{5/2}$ absorption band of Nd^{3+}.

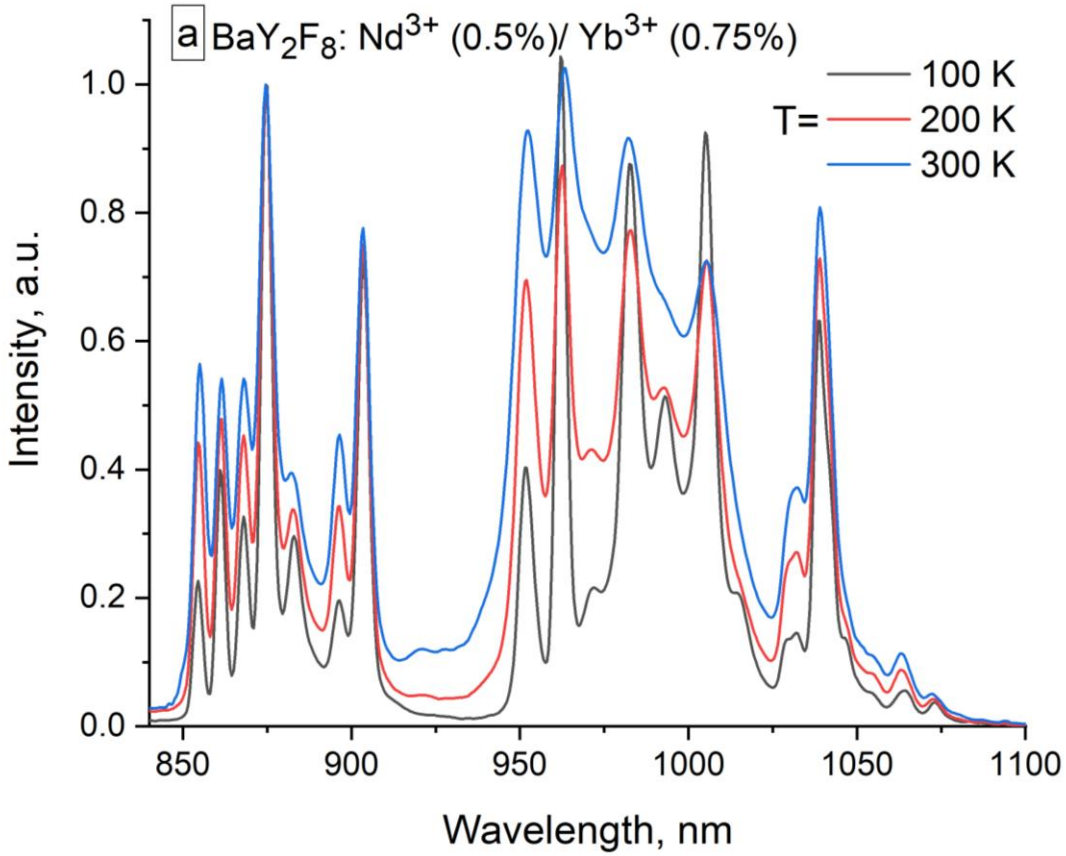
a
BaY2F8: Nd3+ (0.5%)/ Yb3+ (0.75%)
T=
100 K
200 K
300 K
Intensity, a.u.
Wavelength, nm
0.0
0.2
0.4
0.6
0.8
1.0
850
900
950
1000
1050
1100

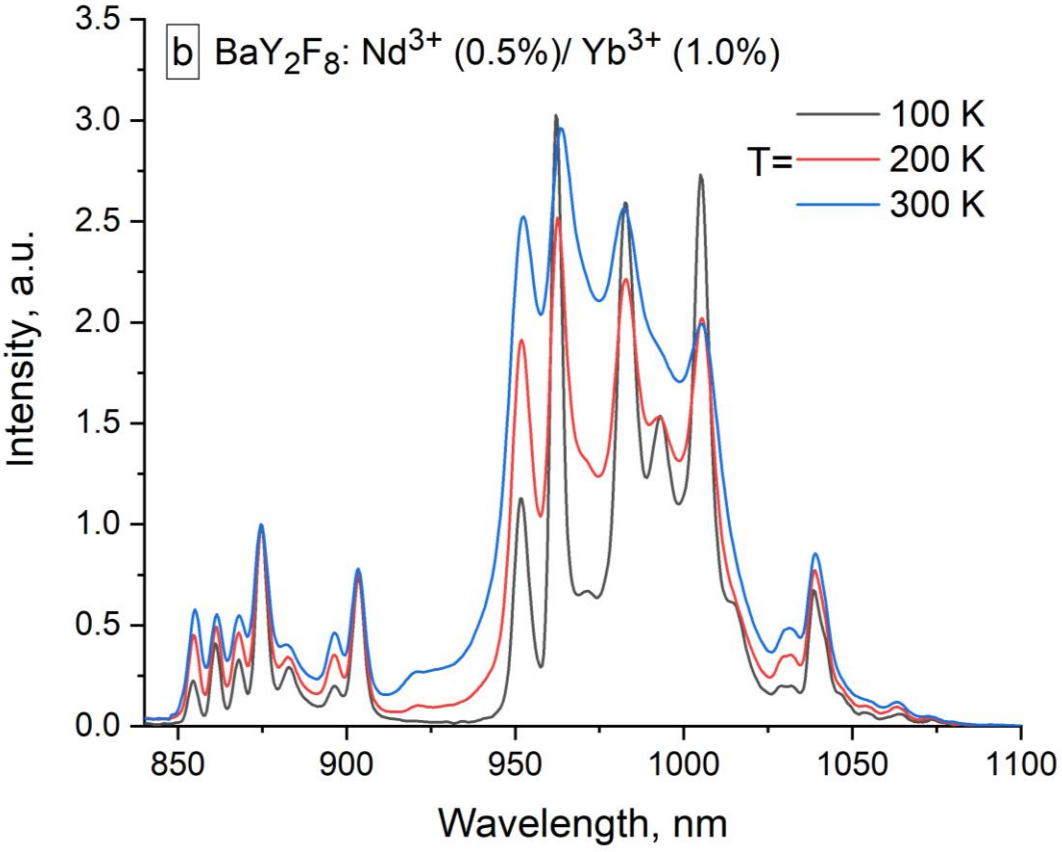
b
BaY2F8: Nd3+ (0.5%)/ Yb3+ (1.0%)
T=
100 K
200 K
300 K
Intensity, a.u.
Wavelength, nm
0.0
0.5
1.0
1.5
2.0
2.5
3.0
3.5
850
900
950
1000
1050
1100

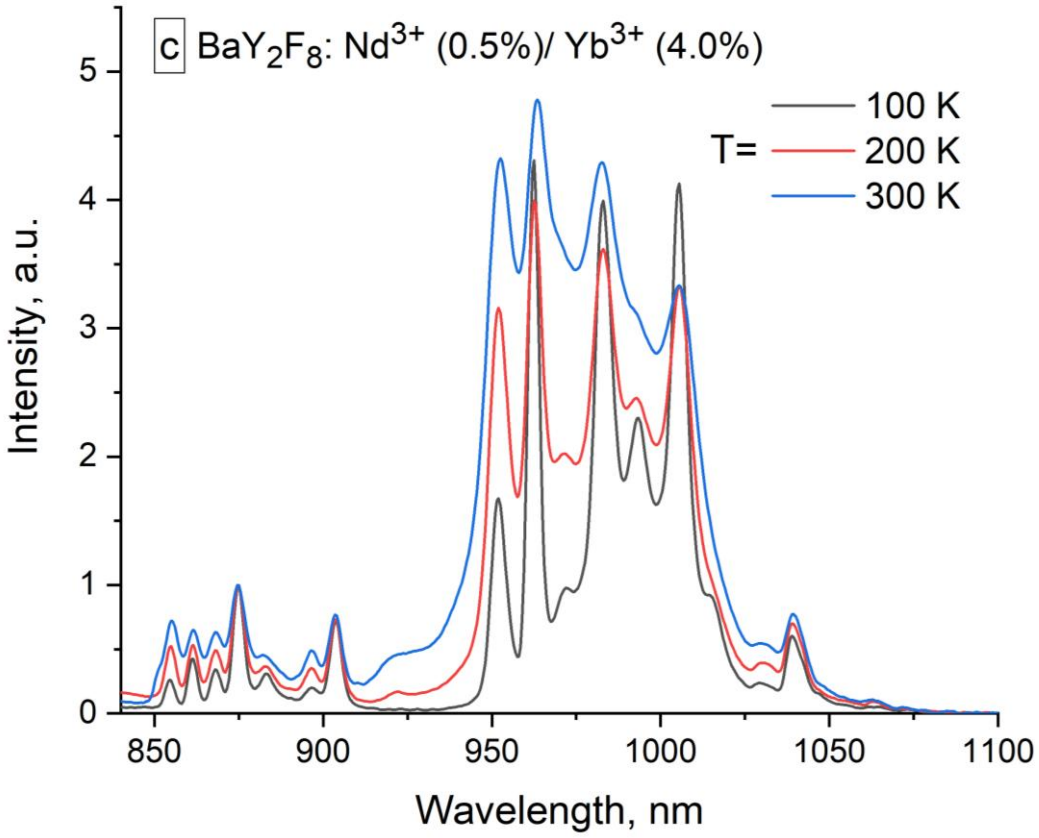

Figure 9. Luminescence spectra of BaY_2F_8:Nd^{3+} (0.5 %)/Yb^{3+} (0.75 %) microparticles in the 100 – 300 K temperature range normalized at 875 nm Stark peak of Nd^{3+}. Excitation wavelength 790 nm corresponds to the $^4I_{9/2}$ – $^4F_{5/2}$ absorption band of Nd^{3+}

It can be seen, that under the 790 nm excitation of Nd^{3+}, the intense Yb^{3+} emission is clearly observed. This fact points to an efficient energy transfer from Nd^{3+} to Yb^{3+}. Moreover, the spectra display almost equal peak intensities of both doping ions which are very convenient for ratiometric temperature sensing. **Figure 9** shows, that the shape of the BaY_2F_8:Nd^{3+} (0.5 %)/Yb^{3+} (0.75 %) microparticle spectrum notably depends on temperature. Specifically, both Nd^{3+} and Yb^{3+} ions demonstrate distinguishable Stark peaks. For each f-f peaks, the intensity of the Stark peaks of the f-f peaks from the short waves increases with the temperature increase. For example, at 320 K Yb^{3+} Stark peak at ~ 953 nm is more intense compared to the peak at 1100 nm. At 80 K, the tendency is opposite. It can be explained by the Boltzmann mechanism of population of higher energy levels. In order to discuss the

spectrum shape behavior we calculated the luminescence intensity ratio (LIR) as a function of temperature according to the formula:

$$LIR = \frac{{}^4F_{\frac{3}{2}} \rightarrow {}^4I_{\frac{9}{2}}(Nd^{3+})}{{}^2F_{\frac{5}{2}} \rightarrow {}^2F_{\frac{7}{2}}(Yb^{3+})}, \qquad (3)$$

The LIR functions of temperature are presented in **Figure 10.**

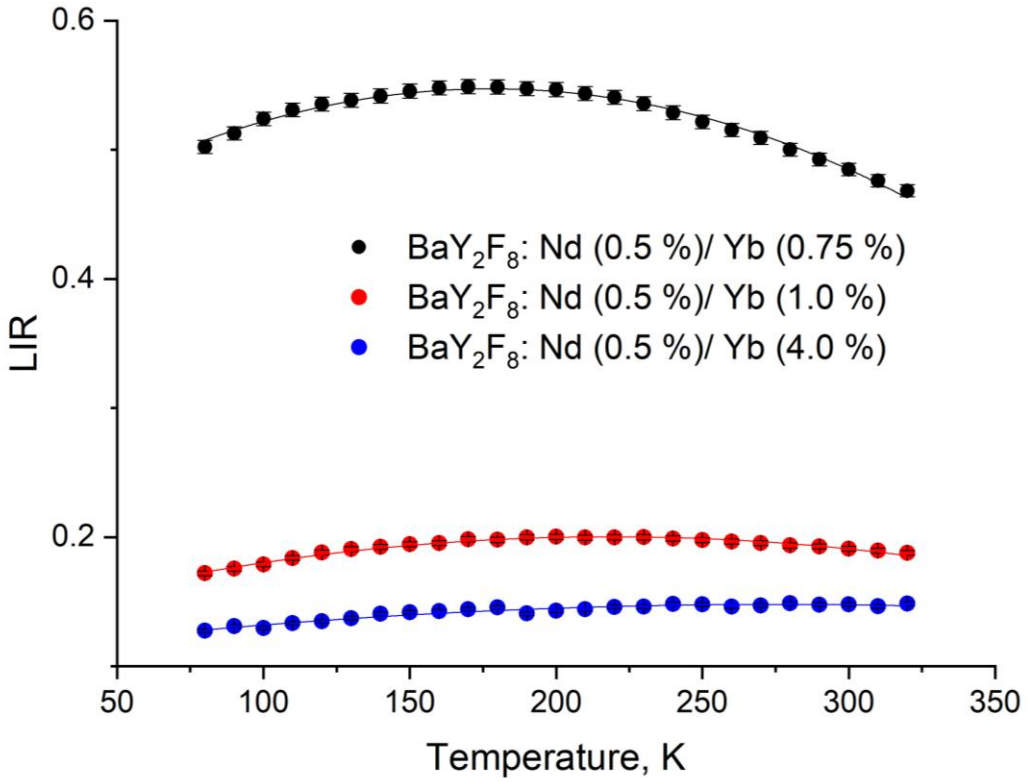

Figure 10. LIR functions of temperature of BaY_2F_8:Nd^{3+} (0.5 %)/Yb^{3+} (0.75, 1.0, and 4.0 %) samples

According to **Figure 10**, the LIR functions display different temperature dependencies. In particular, both BaY_2F_8:Nd^{3+} (0.5 %)/Yb^{3+} (0.75 and 1.0 %) demonstrate the increasing (~ 80 – 200 K) and decreasing (~ 200 – 320 K) parts. In turn, BaY_2F_8:Nd^{3+} (0.5 %)/Yb^{3+} (4.0 %) demonstrate increasing character of the LIR function in the ~ 80 – 250 K range. For higher temperature LIR dependence is almost constant. The temperature evolution of the luminescence peaks **(Figure 9)** revealed that the peak intensity of the normalized spectra does not change such significantly as we observed for YF_3:Nd^{3+}/Yb^{3+} samples. The shape of the peaks changes mostly due to the Stark peaks broadening with the temperature increase.

According to the literature data, the LIR function (I_{Nd}/I_{Yb}) of Nd^{3+}/Yb^{3+} doped inorganic phosphors display decreasing character with the increase of temperature [25]. It can be explained by the fact that the possibility of the phonon-assisted energy transfer increases with the temperature increase. Hence, the depopulation of $^4F_{3/2}$ level (Nd^{3+}) by Yb^{3+} increases, in turn, the population of the excited $^2F_{5/2}$ state of Yb^{3+} increases. Finally, the LIR (I_{Nd}/I_{Yb}) function shows a decreasing character. In the present work, the shapes of the LIR functions are more complicated. In particular, the BaY_2F_8:Nd^{3+} (0.5 %)/Yb^{3+} (4.0 %) sample having the highest Yb^{3+} concentration displays increasing character. It can be explained, that the Yb^{3+} ions form clusters in which the Yb^{3+} luminescence quenching is more efficient. In this case, the Nd^{3+} luminescence decreases due to the energy transfer to Yb^{3+}, in turn, Yb^{3+} luminescence decreases faster with the temperature due to the above-mentioned quenching in clusters. In this case, the I_{Nd}/I_{Yb} ratio (LIR) decreases in the whole temperature range. For the lower Yb^{3+} concentrations, the Yb^{3+} quenching in the clusters is less efficient at higher temperatures, and the LIR function demonstrates decreasing character. The luminescence decay time curves for both Nd^{3+} and Yb^{3+} in the 100 – 300 K temperature range are presented in **Figure S4** of supplementary file.

It should be noted that in the case of temperature sensitivity, both Nd^{3+} and Yb^{3+} have a relatively large energy gap between their $^4F_{3/2}$ and $^2F_{5/2}$ excited states and the lower states. Taking into consideration relatively low phonon energy of BaY_2F_8 host (~ 350 – 380 cm^{-1}) [38] there is a low probability of multiphonon relaxation from the above-mentioned excited states. Hence, the thermal quenching is ineffective at least in the considered 80 – 320 K temperature range. On the other hand, in ion clusters, the excitation energy migrates among homonymous ions until is quenched by the defects.

Interestingly, all the curves showcased very weak temperature dependency compared to our previous work for YF_3:Nd^{3+}/Yb^{3+} [39] or $LiYF_4$:Tm^{3+}/Yb^{3+} [26] samples. Probably, such weak dependence is related to the high probability of the back energy transfer from Yb^{3+} to Nd^{3+} due to the low $^4F_{3/2}$ (Nd^{3+}) $^2F_{5/2}$ (Yb^{3+}) energy gap (~500 cm^{-1}) compared to the energy of phonons in BaY_2F_8 host. These

speculations are in agreement with the temperature-dependent spectral characteristics where the peak intensities of Nd^{3+} and Yb^{3+} did not changed significantly.

Finally, the BaY_2F_8:Nd^{3+} (0.5 %)/Yb^{3+} (4.0 %) sample is the most favorable because here a particular value of the LIR corresponds to a particular value of temperature unlike the bow-shaped LIR functions for BaY_2F_8:Nd^{3+} (0.5 %)/Yb^{3+} (0.75 and 1.0 %) samples. However, in the physiological temperature range for biomedical application, these LIR peculiarities are not important. Anyway, we calculated such important performances as absolute (S_a) and relative (S_r) sensitivities acceding to the equations:

$$S_a = \frac{d(LIR)}{dT}, \quad (4)$$

$$S_r = \frac{1}{LIR} \times \left|\frac{d(LIR)}{dT}\right| \times 100\%, \quad (5)$$

The sensitivities are presented in **Figures 11a** and **11b.**

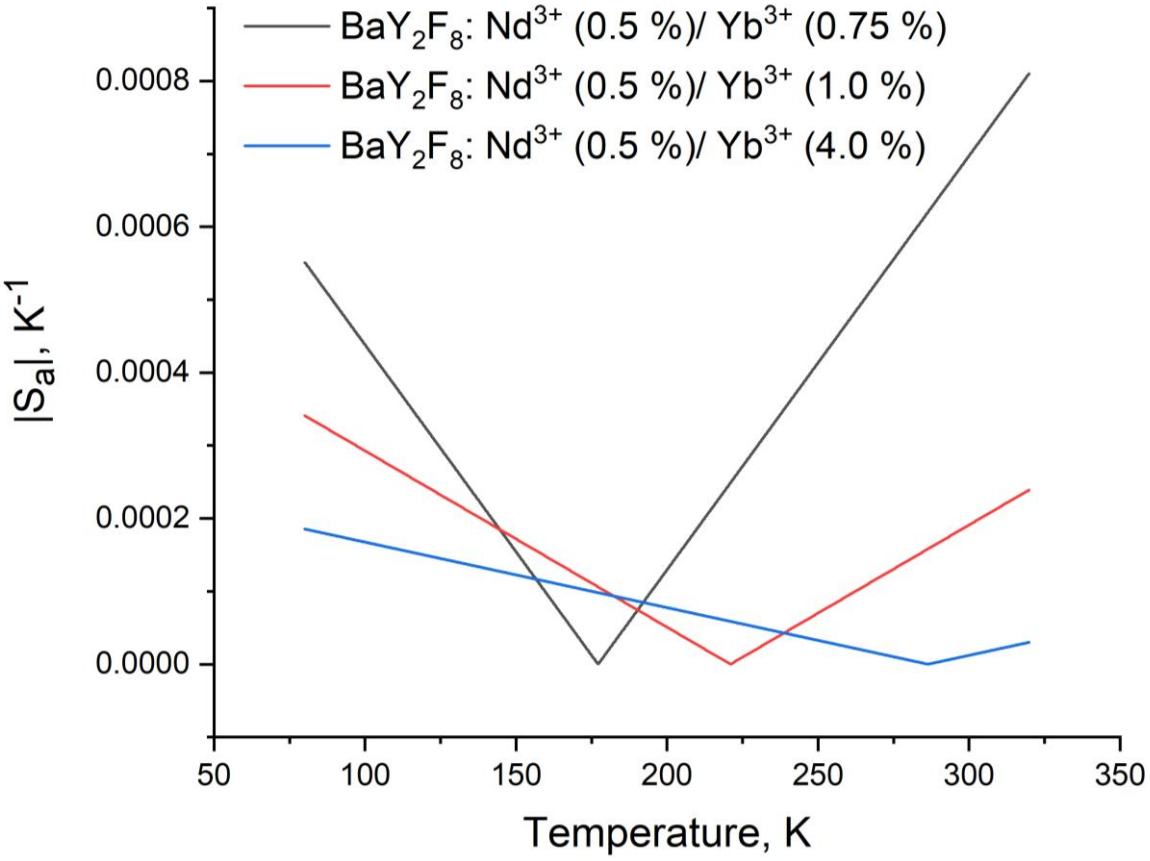

(a)

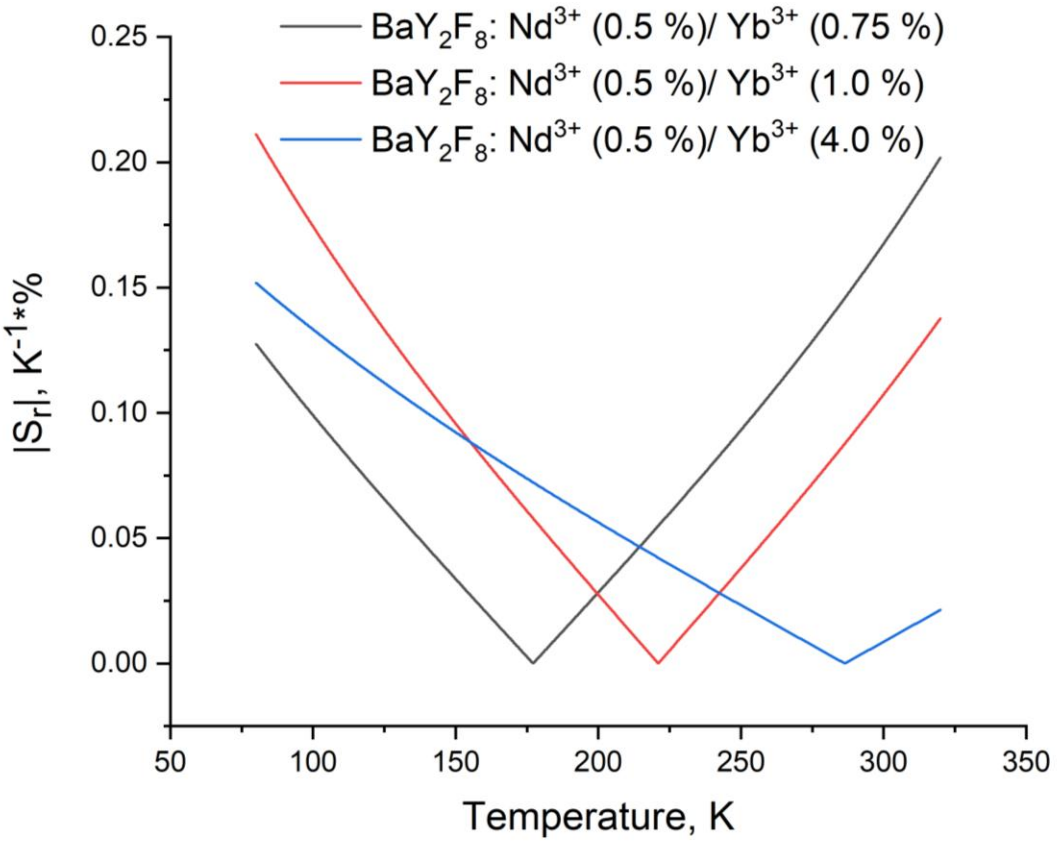

(b)

Figure 11. Absolute (S_a) and relative (S_r) sensitivities of the BaY_2F_8:Nd^{3+} (0.5 %)/Yb^{3+} (0.75, 1.0 and 4.0 %) samples

It can be seen, that the estimated minimums of S_a and S_r reflect the LIR tendencies. Indeed, in the LIR function, the temperature ranges where the LIR function is constant shift toward higher temperatures with the increase of Yb^{3+} concentration (Figure 10). The samples display quite competitive performances compared to the modern world analogs. As we mentioned above, for the BaY_2F_8 system, the Stark peaks of both Nd^{3+} and Yb^{3+} are more pronounces compared to the other fluoride or oxide matrices. In this case, the LIR function based on Stark peaks can be more sensitive temperature-dependent parameter. The Stark peaks were interpreted according to the literature data [37]. Indeed, the Nd^{3+} ratiometric luminescence thermometry based on the ratio of Nd^{3+} Stark peaks was successfully investigated earlier [15], [8]. Here, the competitive relative temperature sensitivities

were obtained at room temperature and higher. Here, we demonstrate a slightly new approach. Since the Stark peaks of both Nd^{3+} and Yb^{3+} are well-reserved (especially around liquid nitrogen temperatures), the LIR based of I_{Nd}/I_{Yb} Stark peaks can be realized.

The $^4F_{3/2}$ excited state of Nd^{3+} is split into two Stark components sharing their electron population according to the Boltzmann law (2^{th} – the highest 1^{th} the lowest). In turn, the $^2F_{5/2}$ excited state of Yb^{3+} has three Stark components (from the 1^{th} the lowest to 3^{th} the highest). It is well-known, that the populations of the higher Stark levels increase with the temperature increase. The lower Stark levels demonstrate an opposite tendency. Thus, the emission intensities from higher Stark levels increases while the emissions from the lower ones decreases. In order to gain the higher temperature sensitivities, we need to take the ratio of two peaks having the opposite temperature behavior (**Figure 12**).

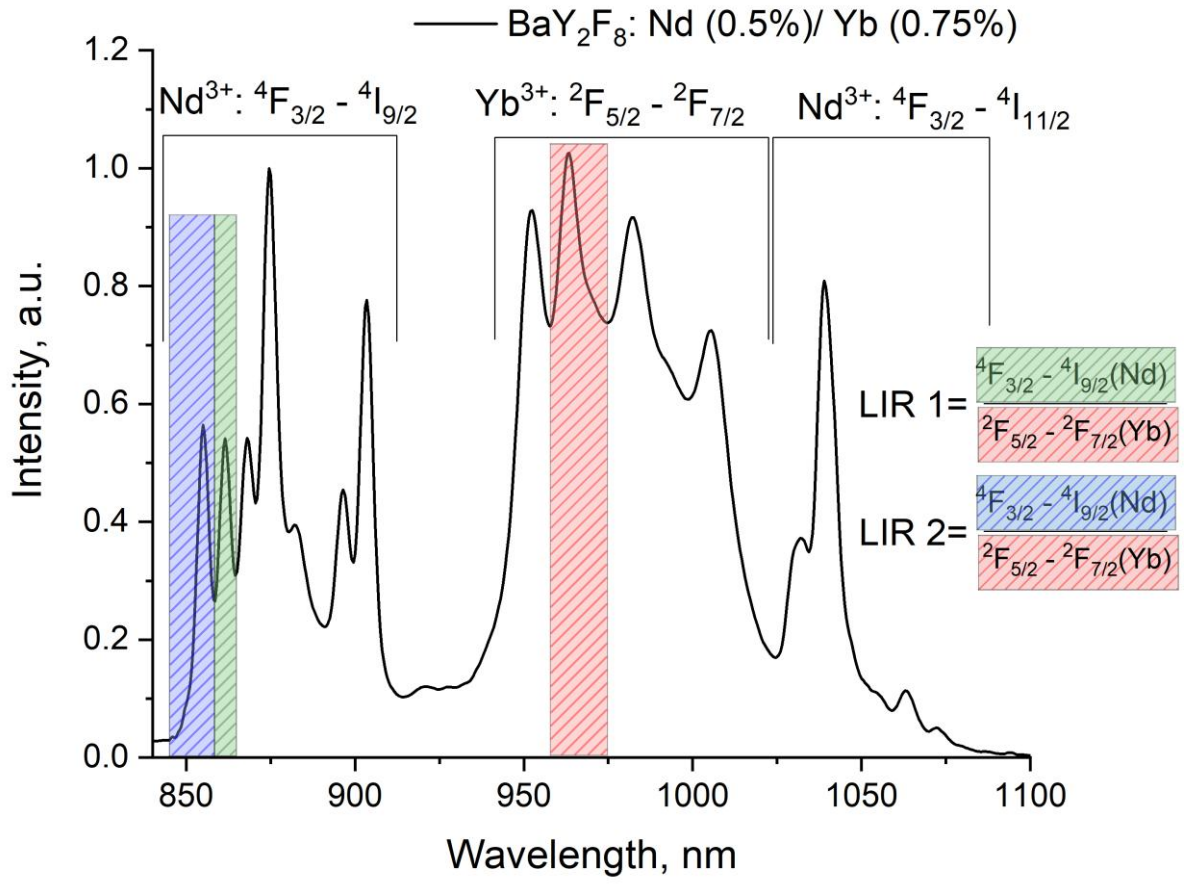

Figure 12. The definition of two LIR functions: LIR1 – 1th of Nd^{3+} to 1th of Yb^{3+} and LIR2 – 2th of Nd^{3+} to 1th of Yb^{3+} BaY_2F_8:Nd^{3+}(0.5 %)/Yb^{3+} (0.75 %) sample

However, we also compare LIRs base of the lowest Stark of Nd^{3+} and the lowest Yb^{3+} one (LIR1) as well as highest Stark of Nd^{3+} and the lowest Yb^{3+} one (LIR2). We made these calculations for the 0.75 and 4.0 % of Yb^{3+}.

Both LIR functions are represented in **Figure 13a** and **13b**.

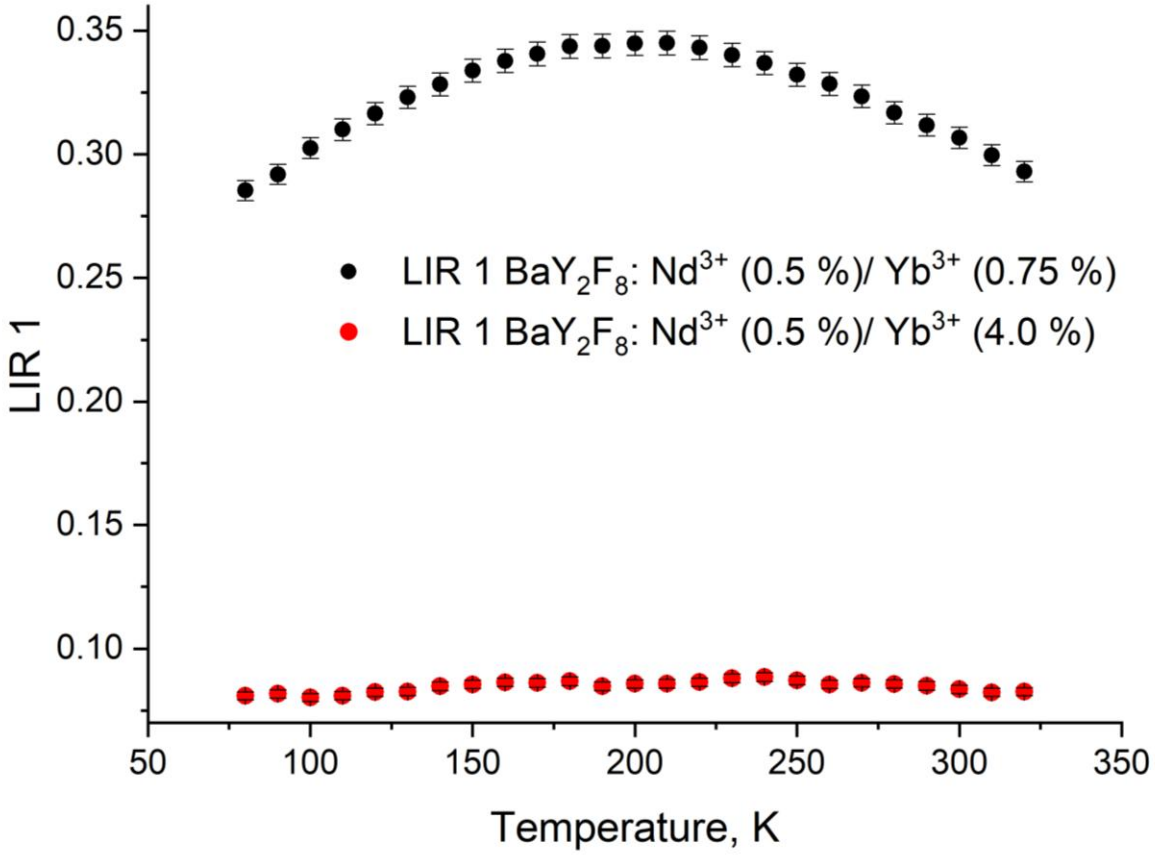

(a)

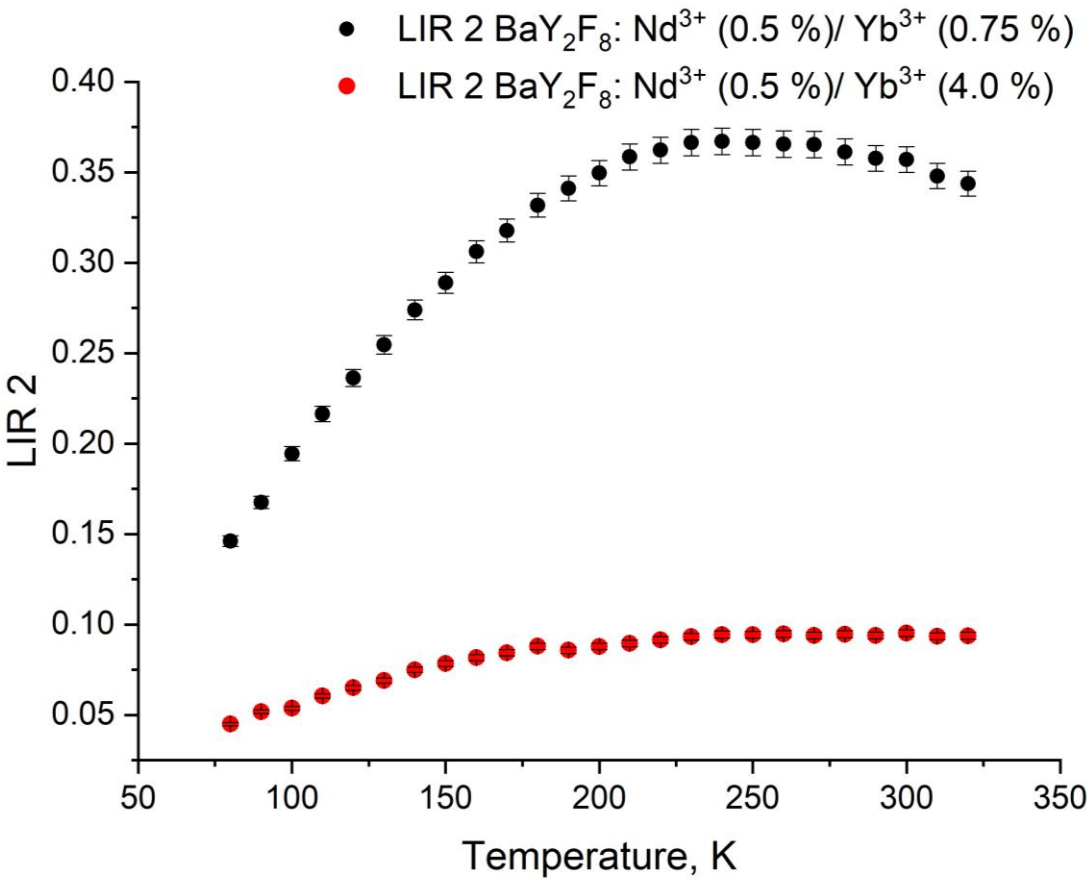

(b)

Figure 13. The LIR functions: LIR1 – 1th of Nd^{3+} to 1th of Yb^{3+} and LIR2 – 2th of Nd^{3+} to 1th of Yb^{3+} of both BaY_2F_8:Nd^{3+}(0.5 %)/Yb^{3+} (0.75 and 4.0 %) sample

Indeed, it can be seen, that the LIR2 (highest Nd^{3+} Stark divided by the lowest Yb^{3+} one) function displays more pronounced temperature dependency especially in the cryogenic temperature range. In the case of LIR2, the function is increasing with a saturation part. Indeed, the population of the highest Nd^{3+} Stark level increase with the temperature while the population of the lowest Yb^{3+} one decreases.

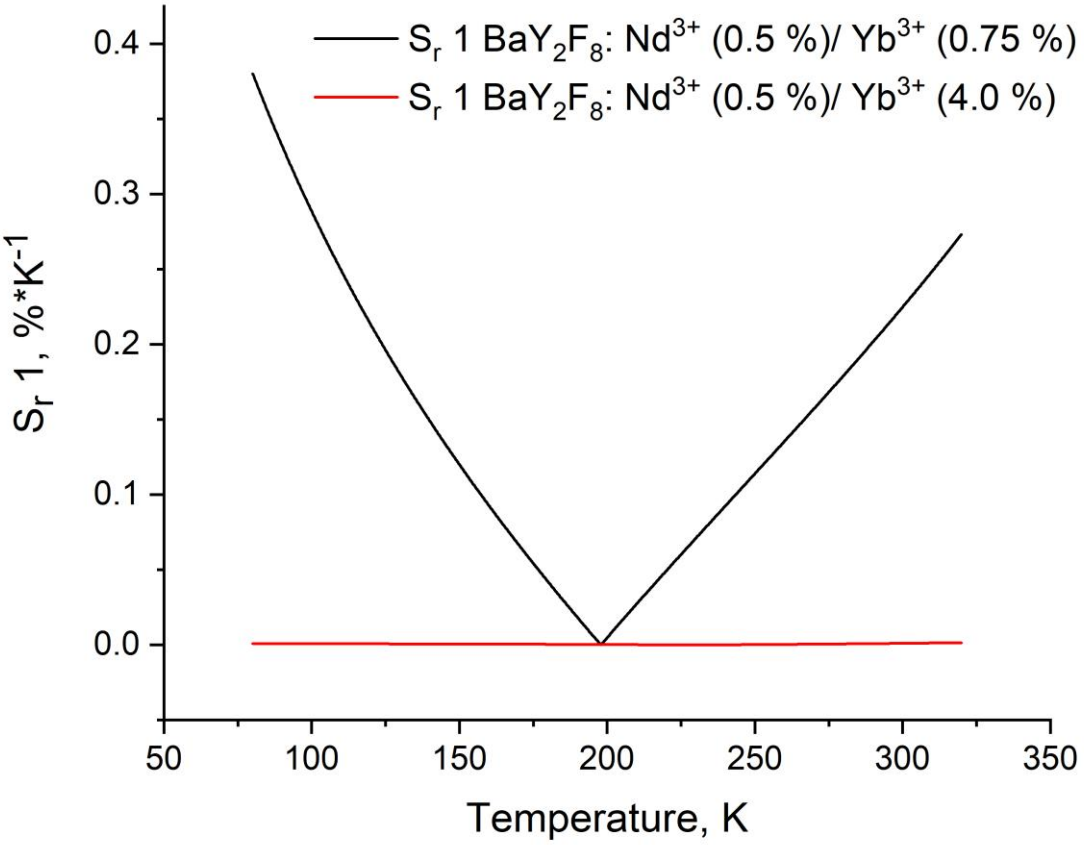
S_r 1 BaY_2F_8: Nd^3+ (0.5 %)/ Yb^3+ (0.75 %)
S_r 1 BaY_2F_8: Nd^3+ (0.5 %)/ Yb^3+ (4.0 %)
S_r 1, %*K^-1
0.4
0.3
0.2
0.1
0.0
50
100
150
200
250
300
350
Temperature, K

(a)

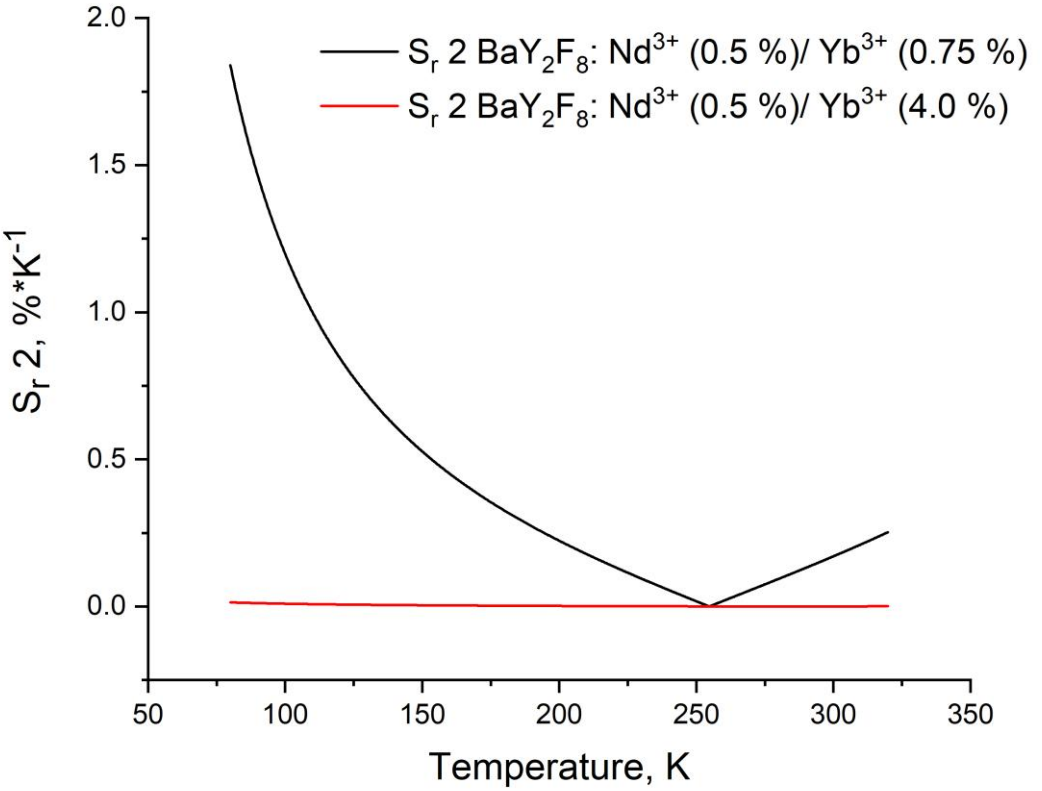

(b)

Figure 14. The S_r plots based on the LIR of Nd^{3+} and Yb^{3+} Stark peaks

It can be seen, that the highest values of the sensitivities are in the liquid nitrogen temperature range. In addition, the LIR2 functions displayed the highest temperature sensitivities. It can also be seen, that the sample having the lowest Yb^{3+} concentration (0.75 %) showed the higher sensitivities. The observed phenomenon requires additional investigations. However, it can be suggested, that as it was mentioned above, at the higher Yb^{3+} concentrations these ions form pairs or clusters. Here, the probability of the energy diffusion between Yb^{3+} is higher. It also diminishes the probability of the Nd^{3+} - Yb^{3+} back energy transfer. Thus, in 0.75 % of Yb^{3+} sample the $^4F_{3/2}$ excited state of Nd^{3+} is additionally populated by Yb^{3+}, and the emission from this excited state (the highest Nd^{3+} Stark level) in more intense and it grows faster with the temperature because of both Boltzmann process and the BET. In the case of 4.0 % of Yb^{3+}, the effectiveness of W_{BET} is less, hence, the highest Nd^{3+} Stark level in populated by only the lowest one. Thus, the $I_{Stark\_Nd}/I_{Stark\_Yb}$ (LIR2) of

BaY_2F_8:Nd^{3+} (0.5 %)/Yb^{3+} (0.75 %) sample showed more pronounced dependency on temperature compared to the LIR2 of BaY_2F_8:Nd^{3+} (0.5 %)/Yb^{3+} (4.0 %) sample.

The comparison of the obtained values of temperature sensitivity is presented in **Table 3.**

Table 3. The comparison of the obtained values of temperature sensitivity with the world analogs

Sample	λ_{exc}, nm	Temperature range, K	Emission lines for LIR, nm	S_r, %*K^{-1}	Ref.
Y_2O_3: Nd^{3+}/ Yb^{3+}	804	289-328	1055/976	0.48	[16]
$Y_2Al_5O_{12}$: Nd^{3+}/ Yb^{3+}			1051/965.9	0.33	
$Y_2Ge_2O_7$: Nd^{3+}/ Yb^{3+}			1056/978	0.22	
YBO_3: Nd^{3+}/ Yb^{3+}			1056/971	0.21	
Y_3BO_6: Nd^{3+}/ Yb^{3+}			1072/977	0.18	
YF_3: Nd^{3+}/Yb^{3+}	790	80-320	866/986	0.1-0.4	[14]
$LuVO_4$: Nd^{3+}/Yb^{3+}	808	123-573	1060/975	0.34	[40]
$NaYF_4$:Nd^{3+}-Yb^{3+}/$NaYF_4$/ $NaYF_4$:Er^{3+}-Yb^{3+}	980	303-423	805/655, 865/655	4.3, 2.4	[41]
BaY_2F_8: Nd^{3+}, Yb^{3+}	790	80-320	854/963	1.8	This work
$Y_2Ba_3B_4O_{12}$: Nd^{3+}/Yb^{3+}	808	298-328	897/978	0.31	[42]

In order provide further thermometer performances we calculated temperature uncertainly. Temperature uncertainty (or temperature resolution) δT describes the minimum resolvable temperature difference, which depends not only on the material properties but also on the experimental setup. The uncertainty in temperature determination is influenced by several factors, including the measurement system,

experimental conditions, and signal-to-noise ratio. Typically, the temperature uncertainty is estimated using the following formula [4]:

$$\delta T = \frac{1}{S_r}\frac{\delta LIR}{LIR}, \quad (6)$$

The determination of δLIR is presented in the Chapter 2 of the Supplementary file. The temperature uncertainty (δT) for the best BaY_2F_8:Nd^{3+} (0.5%)/Yb^{3+} (0.75 %) sample is presented in **Figure 15**.

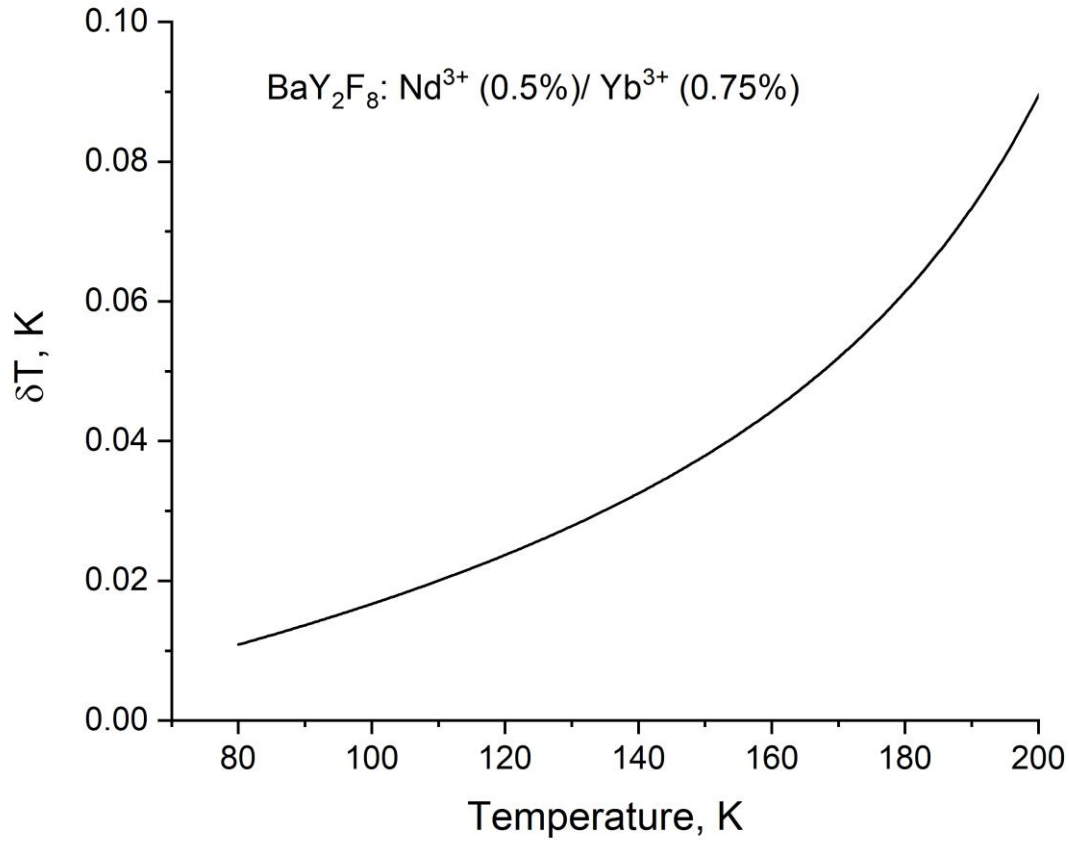

Figure 15. The temperature uncertainty (δT) for the best BaY_2F_8:Nd^{3+} (0.5 %)/Yb^{3+} (0.75 %) sample

No less important performances of the phosphors are photostability and repeatability. For the sake of their determination, spectral and kinetic characterization was performed under continuous laser radiation with a wavelength of 790 nm for an hour every 15 minutes. The results on the photostability of the samples are shown in

the figures. It can be seen, that both spectral and kinetic characteristics are stable under laser radiation at least for an hour. The repeatability was confirmed by several cooling-heating cycles with further calculation of LIR2 as a temperature-dependent parameter. The results are shown in the **Figure S5**.

Conclusions

In this work, we presented experimental results of the spectral-kinetic characterization of BaY_2F_8:Nd^{3+} (0.5 %)/Yb^{3+} (0.75, 1.0 and 4.0 %) microparticles obtained by the mechanical milling of the corresponding bulk crystals. All the samples demonstrated the desired monoclinic crystal structure. The spectral-kinetic characterization revealed an effective energy transfer from Nd^{3+} to Yb^{3+}. By means of EPR spectroscopy, it was found that for single sites of doped ions, g-values of Nd^{3+} and Yb^{3+} ions in the studied powders, agree well with g-values obtained for BaY_2F_8 crystals in literature. In addition, the clear indication of clustering of Yb^{3+} ions was detected in EPR spectra. This is related to the line with g~2.34, which increased considerably for the sample doped with 4.0 % of Yb^{3+} ions. The spectral characterization of the samples in the 80 – 320 K temperature range showed, that the spectral shape is notably dependent on temperature. The peak intensities did not display strong dependence, however, the Stark peaks of both Nd^{3+} and Yb^{3+} showed changes of intensities with the rise of temperature. We took the Stark peaks from the highest Nd^{3+} and the lowest Yb^{3+} Stark levels, because their populations should demonstrate opposite behavior with the increase of temperature. Indeed, the highest Nd^{3+} Stark level is populated more efficiently with the increase of temperature. In turn, the lowest Yb^{3+} one displays inverse trend. The maximum S_r value was 1.8 $\%\cdot K^{-1}$ at 80 K using BaY_2F_8:Nd^{3+} (0.5 %)/Yb^{3+} (0.75 %) sample. The BaY_2F_8:Nd^{3+} (0.5 %)/Yb^{3+} (4.0 %) having the highest Yb^{3+} concentration showed less values of temperature sensitivity. We suggested, that it was related to the raised probability of energy diffusion between Yb^{3+} ions at higher Yb^{3+} concentrations.

Funding

The research was funded by the subsidy allocated to Kazan Federal University for the state assignment in the sphere of scientific activities (FZSM-2025-0004).

Declaration of competing interest

The authors declare that they have no known competing financial interests or personal relationships that could have appeared to influence the work reported in this paper.

References

[1] Y Chen, Y., Li, C., Yang, T., Ekimov, E. A., Bradac, C., Ha, S. T., ... & Tran, T. T. Real-time ratiometric optical nanoscale thermometry, ACS nano 17(3) (2023) 2725-2736, doi: 10.1021/acsnano.2c10974.

[2] Brites, C. D., Lima, P. P., Silva, N. J., Millán, A., Amaral, V. S., Palacio, F., & Carlos, L. D. Thermometry at the nanoscale, Nanoscale 4(16) (2012) 4799-4829, doi: 10.1039/c2nr30663h.

[3] Jaque, D., & Vetrone, F. Luminescence nanothermometry, Nanoscale 4(15) (2012) 4301-4326, doi: 10.1039/c2nr30764b.

[4] Brites, C. D., Marin, R., Suta, M., Carneiro Neto, A. N., Ximendes, E., Jaque, D., & Carlos, L. D. Spotlight on luminescence thermometry: basics, challenges, and cutting-edge applications, Advanced Materials 35(36) (2023) 2302749, doi: 10.1002/adma.202302749.

[5] C Brites, C. D., Balabhadra, S., & Carlos, L. D. Lanthanide-based thermometers: at the cutting-edge of luminescence thermometry, Advanced Optical Materials 7(5) (2019) 1801239, doi: 10.1002/adom.201801239.

[6] Cui, H., Cao, Y., Zhang, Y., Cao, L., Ran, S., Wang, X., ... & Chen, B. Extremely intense green up-conversion luminescent and ultra-high temperature sensitivity in Er3+/Yb3+ co-doped BiTa7O19 phosphors, Journal of Luminescence 241 (2022) 118484, doi: 10.1016/j.jlumin.2021.118484.

[7] Li, L., Cao, Y., Zhang, Y., Cui, H., Li, G., Zhang, J., ... & Chen, B. Excellent upconversion luminescence intensity in Er3+/Yb3+/Mo4+ triple-doped BiTa7O19 phosphors, Journal of Alloys and Compounds 938 (2023) 168725. doi: 10.1016/j.jallcom.2023.168725.

[8] Balabhadra, S., Debasu, M. L., Brites, C. D., Nunes, L. A., Malta, O. L., Rocha, J., ... & Carlos, L. D. Boosting the sensitivity of Nd3+-based luminescent nanothermometers, Nanoscale 7(41) (2015) 17261-17267, 2015, doi: 10.1039/c5nr05631d.

[9] I Kolesnikov, I. E., Kalinichev, A. A., Kurochkin, M. A., Mamonova, D. V., Kolesnikov, E. Y., Kurochkin, A. V., ... & Mikhailov, M. D. New strategy for thermal sensitivity enhancement of Nd3+-based ratiometric luminescence thermometers, Journal of Luminescence 192 (2017) 40-46, doi: 10.1016/j.jlumin.2017.06.024.

[10] Joubert, M. F., Jacquier, B., Linares, C., & Macfarlane, R. M. A spectroscopic study of BaY2F8: Nd3+, Journal of luminescence 47(6) (1991) 269-280.

[11] Shang, F., Hu, C., Xu, W., Zhu, X., Zhao, D., Zhang, W., ... & Cao, W. Near-infrared emitting Nd3+-Yb3+ codoped Y2O3 nanocrystals for highly sensitive optical thermometry. Journal of Alloys and Compounds 858 (2021) 157637. doi: 10.1016/j.jallcom.2020.157637.

[12] Tai, Y., Li, X., & Pan, B. Efficient near-infrared down conversion in Nd3+-Yb3+ co-doped transparent nanostructured glass ceramics for photovoltaic application, Journal of Luminescence 195 (2018) 102-108, doi: 10.1016/j.jlumin.2017.10.051.

[13] Marciniak, L., Bednarkiewicz, A., Trejgis, K., Maciejewska, K., Elzbieciak, K., & Ledwa, K. Enhancing the sensitivity of a Nd3+, Yb3+:YVO4 nanocrystalline luminescent thermometer by host sensitization, Physical Chemistry Chemical Physics 21(20) 2019 10532-10539. doi: 10.1039/c9cp01806a.

[14] Pudovkin, M., Oleynikova, E., Kiiamov, A., Cherosov, M., & Gafurov, M. Nd3+, Yb3+: YF3 optical temperature nanosensors operating in the biological windows, Materials 16(1) (2022) 39. https://doi.org/10.3390/ma16010039

[15] Kolesnikov, I. E., Afanaseva, E. V., Kurochkin, M. A., Vaishlia, E. I., Kalinichev, A. A., Kolesnikov, E. Y., & Lahderanta, E. Upconverting NIR-to-NIR LuVO4: Nd3+/Yb3+ nanophosphors for high-sensitivity optical thermometry. ACS Applied Materials & Interfaces 14(1) (2022) 1757-1764., doi: 10.1021/acsami.1c20937.

[16] Barbosa, I. V., Maciel, C. V., Moura, A. L., Maia, L. J., Ibanez, A., & Dantelle, G. Impact of the nature of oxide host matrices on the thermometric luminescence properties of Nd3+-Yb3+ codoped nanocrystals, Optical Materials 150 (2024) 115143, doi: 10.1016/j.optmat.2024.115143.

[17] Gharouel, S., Labrador-Páez, L., Haro-González, P., Horchani-Naifer, K., & Férid, M. Fluorescence intensity ratio and lifetime thermometry of praseodymium phosphates for temperature sensing, Journal of Luminescence 201 (2018) 372-383, doi: 10.1016/j.jlumin.2018.04.035.

[18] Pudovkin, M. S., Zelenikhin, P. V., Shtyreva, V. V., Evtugyn, V. G., Salnikov, V. V., Nizamutdinov, A. S., & Semashko, V. V. Cellular uptake and cytotoxicity of unmodified Pr3+: LaF3 nanoparticles, *Journal of Nanoparticle Research 21*(8) (2019) 184. https://doi.org/10.1007/s11051-019-4628-9.

[19] P Fedorov, P. P., Luginina, A. A., Kuznetsov, S. V., & Osiko, V. V. Nanofluorides. Journal of Fluorine Chemistry, 132(12) (2011) 1012-1039. doi: 10.1016/j.jfluchem.2011.06.025.

[20] Fedorov, P. P., Semashko, V. V., & Korableva, S. L. Lithium rare-earth fluorides as photonic materials: 1. Physicochemical characterization. Inorganic Materials, 58(3) (2022) 223-245. doi: 10.1134/S0020168522030049.

[21] J Meijer, J. M., Aarts, L., van der Ende, B. M., Vlugt, T. J., & Meijerink, A. Downconversion for solar cells in YF3: Nd3+, Yb3+. Physical Review B—Condensed Matter and Materials Physics, 81(3) (2010) 035107, doi: 10.1103/PhysRevB.81.035107.

[22] Ximendes, E. C., Santos, W. Q., Rocha, U., Kagola, U. K., Sanz-Rodríguez, F., Fernandez, N., ... & Jacinto, C. Unveiling in vivo subcutaneous thermal dynamics by infrared luminescent nanothermometers. Nano letters, 16(3) (2016) 1695-1703, doi: 10.1021/acs.nanolett.5b04611.

[23] Wang, X., Xu, T., Cai, P., Vu, T., & Seo, H. J. Controlled synthesis, multicolor luminescence, and optical thermometer of bifunctional NaYbF4: Nd3+@ NaYF4: Yb3+ active-core/active-shell colloidal nanoparticles. Journal of Alloys and Compounds, 691 (2017) 530-536, doi: 10.1016/j.jallcom.2016.08.262.

[24] D Cooper, D. R., Capobianco, J. A., & Seuntjens, J. Radioluminescence studies of colloidal oleate-capped β-Na(Gd, Lu)F4: Ln3+ nanoparticles (Ln= Ce, Eu, Tb). Nanoscale, 10(16) (2018) 7821-7832., doi: 10.1039/c8nr01262h.

[25] Bednarkiewicz, A., Stefanski, M., Tomala, R., Hreniak, D., & Strek, W. Near infrared absorbing near infrared emitting highly-sensitive luminescent nanothermometer based on Nd3+ to Yb3+ energy transfer, Physical Chemistry Chemical Physics 17(37) (2015) 24315-24321., doi: 10.1039/c5cp03861h.

[26] Khadiev, A. R., Korableva, S. L., Ginkel, A. K., Morozov, O. A., Nizamutdinov, A. S., Semashko, V. V., & Pudovkin, M. S. Down-conversion based Tm3+: LiY1-XYbXF4 temperature sensors. Optical Materials, 134 (2022) 113118., doi: 10.1016/j.optmat.2022.113118.

[27] A Kaczmarek, A. M., Kaczmarek, M. K., & Van Deun, R. Er3+-to-Yb3+ and Pr3+-to-Yb3+ energy transfer for highly efficient near-infrared cryogenic optical temperature sensing. Nanoscale 11(3) (2019) 833-837. doi: 10.1039/c8nr08348g.

[28] Momma, K., & Izumi, F. VESTA 3 for three-dimensional visualization of crystal, volumetric and morphology data, Applied Crystallography 44(6) (2011) 1272-1276., doi: 10.1107/S0021889811038970.

[29] X. Wang *et al.*, “Influence of Yb ions concentration on Ho: BaY2F8 crystals emission in the range of 1–3 μm,” *Opt Mater (Amst)*, vol. 109, Nov. 2020, doi: 10.1016/j.optmat.2020.110141.

[30] Z. Kowalski, S. M. Kaczmarek, K. Brylew, and W. Drozdowski, “Radioluminescence as a function of temperature and low temperature thermoluminescence of BaY2F8:Ce and BaY2F8:Nd crystals,” *Opt Mater (Amst)*, vol. 59, pp. 145–149, Sep. 2016, doi: 10.1016/j.optmat.2015.12.047.

[31] Wang, X., Zhang, C., Li, W., Hu, D., Li, S., Lin, H., ... & Su, Z. Effects of Nd ions on the fluorescence properties of Ho: BaY2F8 crystals in the wavelength range of 1–2.5 μm. Journal of Luminescence, 221 (2020) 116927., doi: 10.1016/j.jlumin.2019.116927.

[32] I. N. Kurkin, K. P. Chernov, and Yu. K. Chirkin, Fiz. Tverd. Tela 21,937 (1979) [Sov. Phys. Solid State 21 (1979) 549 .

[33] A. Abragam, B. Bleaney, Electron Paramagnetic Resonance of Transition Ions; Clarendon Press: Oxford, 1970.

[34] Kaczmarek, S. M., Leniec, G., Typek, J., Boulon, G., & Bensalah, A. (2009). Optical and EPR study of BaY2F8 single crystals doped with Yb. Journal of Luminescence, 129(12), 1568-1574.

[35] V. V. S. R.M. Rakhmatullin, M.S. Pudovkin, “EPR evidence of surface paramagnetic defects formation due to annealing of LaF3 nanoparticles,” *Magn. Reson. Solids*, vol. 21, no. 45, pp. 90–95, 2019, doi: 10.26907/mrsej.

[36] Skripka, A., Morinvil, A., Matulionyte, M., Cheng, T., & Vetrone, F. Advancing neodymium single-band nanothermometry, Nanoscale 11(23) (2019) 11322-11330., doi: 10.1039/c9nr02801c.

[37] Yang, F. The spectroscopic investigation of ZnWO4: Yb3+ single crystal. Journal of Materials Research, 27(16) (2012) 2096-2100. doi: 10.1557/jmr.2012.126.

[38] Dantas, J. M., & Lalic, M. V. First-principles study of the electronic structure and optical properties of the pure BaY2F8, Optical Materials 32(12) (2010) 1633-1636. doi: 10.1016/j.optmat.2010.05.013.

[39] Pudovkin, M. S., Ginkel, A. K., Morozov, O. A., Kiiamov, A. G., & Kuznetsov, M. D. Highly-sensitive lifetime optical thermometers based on Nd3+, Yb3+: YF3 phosphors, Journal of Luminescence 249 (2022) 119037, doi: 10.1016/j.jlumin.2022.119037.

[40] Kolesnikov, I. E., Afanaseva, E. V., Kurochkin, M. A., Vaishlia, E. I., Kolesnikov, E. Y., & Lähderanta, E. Dual-center co-doped and mixed ratiometric LuVO4: Nd3+/Yb3+ nanothermometers. *Nanotechnology*, *33*(16) (2022) 165504.

[41] Shang, F., Zhao, C., Zhang, T., Liu, S., Guo, P., Wang, Y., ... & Xu, W. High-performance ratiometric luminescence thermometry based on NaYF4: Nd3+-Yb3+/NaYF4/NaYF4: Er3+-Yb3+ core/shell/shell nanoparticles. *Ceramics International* (2025) https://doi.org/10.1016/j.ceramint.2025.02.137

[42] Ferreira, L. H., & Maia, L. J. Synthesis, structural and temperature-sensing properties of nanosized Y2Ba3B4O12: Nd3+/Yb3+ phosphors, Physica B Condensed Matter 657 (2023) 414825.